Chapter 1

Theoretical background

A cold atom experimentalist draws on a panoply of tools (both conceptual and instrumental) which are all intricate and absorbing in their own right. This chaper presents the essential ideas needed to give form and context to the content of the major works reported in this thesis[1]. We will glance at the Hydrogen atom to establish a language with which to elucidate the deceptively simple structure of Helium. We must be equipped with some study of the coupling between electromagnetic fields and light, given the ubiquitous use of laser sources and magnetic trapping in this dissertation, and the focus[2] on laser spectroscopy. Of course, the fun doesn't end when the lights turn off: Even dark, cold, and dilute helium exhibits important and occasionally explosive two-body interactions, which both pave road towards absolute zero while imposing limits on the size and lifetime of atomic condensates. Finally, we will review the basic features of the emergence of macroscopic coherence in the form of a Bose-Einstein condensate.

1.1 Atomic structure

The discussion in this section is a short tour in atomic physics. Many high-quality textbooks atomic physics go into much greater detail than is required for this thesis. In this section, only the essential points are presented. Some lengthy steps in the calculations are omitted, and references provided for the complete working. What follows largely comes from [29, 9] unless otherwise specified. Let us first briefly consider the Hydrogen atom, so that we can discuss its more complex cousin Helium in sensible terms.

Quantum mechanics is the study of systems whose state at ~~a~~ any time t is completely cified by wavefunction $|\psi(t)\rangle$ and whose dynamics are determined by the time-dependent Schrödinger equation,

$$i\frac{\partial}{\partial t}|\psi(t)\rangle = \hat{H}|\psi(t)\rangle. \tag{1.1}$$

The wavefunction $|\psi\rangle$ is represented by a *state vector* that is an element of the complex Hilbert space $\mathcal{H}$. The *Born rule* postulates that the probability of a quantum system being observed in the state $|\psi\rangle$ given that it is known to be in the state $|\phi\rangle$ is given by squared inner product $|\langle\psi|\phi\rangle|^2$. States are orthogonal if the inner product is zero, but the system may evolve naturally from $|\phi\rangle$ to have a nonzero projection onto $|\psi\rangle$ under the action of $\hat{H}$. The Hamiltonian $\hat{H}$ is a linear operator with the Hermitian property $\hat{H}^\dagger = H$, where the

[1] A neophyte physicist may feel a compulsion to delve even deeper, under the weight of one's curiosity. It bears reflecting on the caveat that knowledge is not power but potential energy: One has to do real work to realize that potential.

[2] The *focus* of a lens or mirror is the point of maximum concentration of light that is refracted or reflected from a distant or uniform source. Originally, the term referred to the fireplace at the centre of traditional single-room dwellings; still the brightest point of light, but also the source itself.

dagger denotes the conjugate transpose operation. [3] The Hermitian property guarantees $\hat{H}$ is *normal*, $[\hat{H}^\dagger, \hat{H}] = 0$ and therefore the time-independent Schrödinger equation

$$\hat{H}|\psi\rangle = E|\psi\rangle \tag{1.2}$$

specifies the eigenvectors $|e_n\rangle$ of $\hat{H}$ which provide a complete orthonormal basis for $\mathcal{H}$. This allows any (pure) quantum state to be written in the form $|\psi\rangle = \sum_n a_n|e_n\rangle$. An interpretation of this fact in the light of the Born rule is that the energy eigenstates $|e_i\rangle$ correspond to the distinguishable, mutually exclusive states of a system, which can be discriminated from other states by their energy eigenvalue E_i. In the cases where eigenvalues coincide, there exists at least one other observable that distinguishes the energy eigenstates.

Let us consider an atom immersed in an electric field oscillating with frequency $\omega = 2\pi f$ rad Hz, and write the Hamiltonian in the form

$$\hat{H}(t) = \hat{H}_0 + \hat{H}_I(t) \tag{1.3}$$

where the bare atomic Hamiltonian H_0 sets the energy scale of the system, and the monochromatic time-dependent perturbation takes the form $\hat{H}_I(t) = \Lambda\cos(\omega t)$. We will give physical meaning to Λ in a moment. The energy eigenbasis for a single charged particle bound in a central potential[4] have the form,

$$\psi_{nlm}(r,\theta,\phi) = \sqrt{\left(\frac{2}{na_0^*}\right)^3 \frac{(n-l-1)!}{2n(n+l)!}} e^{-\rho/2}\rho^l L_{n-l-1}^{2l+1}(\rho)Y_l^m(\theta,\phi) \tag{1.4}$$

when written in spherical coordinates (r,θ,ϕ), where $\rho = 2r/na_0^*$ and $a_0^* = \frac{4\pi\epsilon_0\hbar^2}{\mu e^2}$ is the reduced Bohr radius. The radial Laguerre polynomials $L_{n-l-1}^{2l+1}(r)$ and the spherical harmonics $Y_{l,m}(\theta,\phi)$ are labeled by the angular momentum l, the magnetic quantum number m, and the energy is fixed by the principal quantum number n as $E_n = -hcR_\infty/n^2$. The bound-state energy E_n is negative - one must do work to ionize the atom and produce the free ion-electron pair whose energy is defined to be zero. The quantum numbers l and m distinguish states that are otherwise degenerate in n, and serve to lift the degeneracy via the Zeeman shift as I discuss in a later section. Here, $h = 2\pi\hbar$ is the Planck constant, ε_0 is the electric permittivity of free space, and μ is the Bohr magneton.

Let us recall that the time-dependent state can be written in terms of the eigenbasis $|\psi_n\rangle$ of $\hat{H}_0$,

$$|\Psi(t)\rangle = \sum_n c_n(t)e^{-i\omega_n t}|\psi_n\rangle, \tag{1.5}$$

where $\omega_n = E_n/\hbar$. Substitution into Eqn 1.1 reduces to the coupled set of differential equations

$$i\hbar\dot{c}_n(t) = \sum_m e^{-i(E_m-E_n)t/\hbar}\langle\psi_m|\hat{H}_I|\psi_n\rangle, \tag{1.6}$$

which can be solved succinctly after making two simplifications. First, let us assume (without loss of generality) that the atom is initially in the state ψ_1, where $c_1(0) = 1$ and $c_i(0) = 0\ \forall i \neq 1$. Then at a time t the probability that the atom is in the state ψ_k is [29, 9]

$$P_k(t) = 4|\langle\psi_k|H_i|\psi_1\rangle|^2 \frac{\sin^2(\frac{1}{2}(\omega_k-\omega)t)}{(\omega_k-\omega)^2}, \tag{1.7}$$

[3] Formally, $\mathcal{H}$ is a vector space $\mathbb{C}^D$ of dimension D which is complete with respect to the L^2 norm $||x|| = \sqrt{\langle x|x\rangle}$ induced by the inner product $\langle x|y\rangle \to \mathbb{C}$, and $\hat{H} \in \mathcal{B}$, the Banach space of bounded linear operators $\hat{O} : \mathcal{H} \to \mathcal{H}$. $\mathcal{B}$ is also a vector space with a norm (the trace norm) but not an inner product. The states themselves are defined up to scalar multiplication, and hence are actually rays in $\mathcal{H}$ better thought of as points in projective space; we will simply assume they are normalized as $\langle\psi|\psi\rangle = 1$ for brevity. We will say no more of the tremendous consternations which stem from the Born rule.

[4] Better known as the hydrogen atom

where $\omega_k = (E_1 - E_k)/\hbar$. An immediate consequence is that the denominator in suppresses excitation into $|\psi_k\rangle$ unless ω is close to the resonant frequency ω_k. This weak driving permits us to make a further simplification and consider an atom with only *two* states, labeled 1 and 2, with a resonant frequency $\omega_0 = (E_2 - E_1)/\hbar$. Further, the numerator captures the essential feature that the state oscillates between states in response to the driving field. We are now ready to impart a physical meaning to the coupling term: An atom exposed to an oscillating field will respond by oscillating between energy eigenstates, each of which having their own charge distribution through space. This produces an oscillating electric dipole whose interaction with the electric field can be simplified by working in the *dipole approximation*: Assume the electric field has a constant value throughout space, but oscillates in time as $\mathbf{E}(t) = \mathbf{E}_0 \mathrm{Re}(e^{-i\omega t}\hat{\varepsilon})$, where $\hat{\varepsilon}$ is the unit polarization vector, and $\mathbf{r} = r\hat{\mathbf{r}}$. The interaction energy is then given by retaining only the dipole operator $-e\mathbf{r}$ from the multipole expansion of the electronic charge distribution[5]. The interaction Hamiltonian can then be written as

$$\hat{H}_I = e\mathbf{r} \cdot \mathbf{E}(t), \tag{1.8}$$

and the excitation probability can be written in the more familiar form [29, 9]

$$P_2(t) = \Omega^2 \frac{\sin^2(\frac{1}{2}(\omega_0 - \omega)t)}{(\omega_0 - \omega)^2}, \tag{1.9}$$

in terms of the Rabi frequency

$$\Omega = \frac{\langle \psi_1 | e\mathbf{r} \cdot \mathbf{E} | \psi_2 \rangle}{\hbar}. \tag{1.10}$$

The dipole operator $-e\mathbf{r}$ inherits the structure of the orbitals, which allows a separation of the expectation value in the preceding equation into radial and angular parts, $\langle 2|\mathbf{r} \cdot \hat{\varepsilon}|1\rangle = \langle 2|R|1\rangle \mathcal{I}$. Setting aside the radial part R, the angular integral $\mathcal{I}$ can be written as a contraction over the spherical harmonic basis functions,

$$\mathcal{I} = \int_0^{2\pi} \int_0^{\pi} Y^*_{l_2,m_2}(\theta,\phi) \hat{r} \cdot \hat{\varepsilon} Y_{l_1,m_1}(\theta,\phi) \sin\theta d\theta d\phi \tag{1.11}$$

is zero unless some constraints, known as *selection rules*, are satisfied. To proceed, we assume that the atom is immersed in a magnetic field and define the z axis to be the direction of the magnetic field vector $\mathbf{B}$[6]. The dipole operator can then be written as the superposition of the linear and circular oscillating field components,

$$\hat{r} \cdot \hat{\varepsilon} \propto A_{\sigma^-} Y_{1,-1} + A_z Y_{1,0} + A_{\sigma^+} Y_{1,+1}, \tag{1.12}$$

where the $A_{\sigma^\pm}$ are the amplitudes of the clockwise- and anti-clockwise circular polarization, and A_z the amplitude of linear polarization in the atomic reference frame. When this expression is inserted into the integral $\mathcal{I}$, the orthogonality of spherical harmonics and the relationship

$$Y_{1,m} Y_{\lambda,\mu} = A Y_{1+\lambda,m+\mu} + B Y_{\lambda-1,m+\mu} \tag{1.13}$$

ensures

$$\Omega \propto a\delta_{l_2,l_1+1}\delta_{m_2,m_1+m} + b\delta_{l_2,l_1-1}\delta_{m_2,m_1+m} \tag{1.14}$$

where $m = \pm 1, 0$ as in the expansion of the dipole operator, and a, b are constants whose exact values are not required here. Thus $\mathcal{I} = 0$ unless $\Delta l = \pm 1$ and either $\Delta m_l = 0$ or $\Delta m_l = \pm 1$. Transitions not satisfying these conditions are said to be *forbidden*, but in reality they still occur, and can be accounted for by including higher terms in the series

[5] This is a good approximation when the wavelength $\lambda = c/f$, fixed by the vacuum speed of light c, is much larger than the atom This is universally applicable for our purposes as the size of the helium atom is $\approx$ 30pm, some 0.1% of the shortest wavelength of light used in this thesis

[6] This is true for almost all the contexts we encounter in this thesis, but where a magnetic axis is not present, one should perform an average over all angles as required.

expansion of the interaction Hamiltonian. Emission or absorption events with $\Delta m_l = 0$ are called π-transitions, and correspond to the dipole moment induced by light with linear polarization along the quantization axis, whose amplitude is captured by the A_z term in Eqn. 1.12. The σ transitions couple to oscillations in the plane normal to the quantization axis, and correspond to transitions where $\Delta m_l = \pm 1$, driven by the $A_{\sigma^\pm}$ terms.

orientation dependence goes here

This description of the coupling between atomic states and the electric field is sufficient, with some further work, to derive the Einstein rate equations for absorption and stimulated emission [29]. However, the more familiar phenomenon of spontaneous emission remains out of reach. requires the full-blown theory of quantum electrodynamics for an explanation, and so we shall not proceed to derive it here. Instead we will have to be satisfied with a classical model which captures some of the essential features so far left unmentioned.

Classical oscillator model

In the *Lorentz oscillator* picture, one approximates an atom by a positive charge fixed at the origin with a harmonically-coupled negative charge with a single degree of freedom $x(t)$ whose potential is zero at $x(t) = 0$. The electron's equation of motion is $\ddot{x} + \Gamma\dot{x} + \omega_0^2 x = -eE(e)/m_e$, where

$$\Gamma = \frac{e^2\omega^2}{6\pi\varepsilon_0 m_e c^3} \tag{1.15}$$

is the damping rate corresponding to radiative decay. The spectrum of an exponentially decaying oscillator has the familiar Lorentzian lineshape,

$$\alpha(\omega) = \frac{6\pi\varepsilon_0 c^3}{\omega_0^2}\frac{\Gamma}{\omega_0^2 - \omega^2 - \mathrm{i}(\omega^3/\omega_0^2)\Gamma}, \tag{1.16}$$

Where the polarizability $\alpha(\omega)$ determines the amplitude of the dipole response via $\mathbf{p}(t) = \alpha(\omega)E(t)$. This reponse function features the characteristic full-width at half-maximum (FWHM) scale of each transition, which is the inverse of the lifetime $\tau = 1/\Gamma$. The interaction energy of the dipole and the electric field is $U_{dip} = -\frac{1}{2}\langle \mathbf{p}\cdot\mathbf{E}\rangle = -\frac{1}{2\varepsilon_0 c}Re(\alpha)I(\mathbf{r})$, which inherits a spatial structure from the intensity $I(\mathbf{r})$. When the polarizability is positive (that is, when the light is red-detuned from ω_0 and the denominator has a positive real part) then the dipole oscillates in-phase with the field and so the interaction energy is minimized at the intensity maxima. This is the operational principle of optical dipole traps, wherein the *dipole force* $F_{dip} = -\nabla U_{dip} \propto \nabla I(\mathbf{r})$ confines atoms to the focus of a laser beam[7]. Ashkin made the first demonstration of the dipole force by trapping micron-sized particles in 1970, and Letokhov suggested 1D confinement of atoms the next year. Ashkin suggested 3D trapping only in 1978, and shortly afterward the dipole force was demonstrated on neutral atoms by Bjorkholm *et al.* 1978. In 1986 Chu *et al.* accomplished the first optical trap, and the first BEC produced exclusively using optical trapping was achieved in 2001 [6]. The dipole force is most pertinent to the works in chapter **??** as it is the basic principle underpinning optical lattice traps.

In the case where the detuning Δ is small in comparison to ω_0 (as will be the case throughout this dissertation), the dipole potential can be written in the form [32]

$$U_{dip}(\mathbf{r}) = \frac{3\pi c^2}{2\omega_0^3}\frac{\Gamma}{\Delta}I(\mathbf{r}), \tag{1.17}$$

and absorption of light is captured by the imaginary part of the polarizability[8], which is related to the scattering rate as

$$\Gamma_{sc} = \frac{\mathrm{Im}(\alpha)I(\mathbf{r})}{\hbar\varepsilon_0 c}. \tag{1.18}$$

[7] the dipole force can also be generated with blue-detuned beams to create repulsive potential barriers

[8] A careful derivation can be found in [29], and an extremely detailed one in [**CohenTannoudji**]

Light scattering competes with the dipole force because repeated absorption of photons with momentum $\hbar k$ at a rate Γ_{sc} gives rise to an effective force of $F_{sc} = \Gamma_{sc}\hbar k$, not to mention the deleterious effects of heating by repeated absorption events. Fortunately, in all situations relevant to our concerns here, the scattering rate can be written

$$\Gamma_{sc}(\mathbf{r}) = \frac{3\pi c^2}{2\hbar\omega_0^3}\left(\frac{\Gamma}{\Delta}\right)^2 I(\mathbf{r}), \tag{1.19}$$

from which it can be seen that $\Gamma_{sc}/U_{dip} \propto \Gamma/\Delta$ - that is, for large enough detuning, the scattering rate is dominated by the dipole force.

Returning to multilevel atoms, a fine way to better approximate the atomic polarizability is to compute the dipole potential of an atom initially in the $|1\rangle$ state by summing over the level shifts associated with transitions to all other states, giving the form

$$\Delta U = \sum_i \frac{|\langle 1|H|i\rangle|^2}{\omega_i}. \tag{1.20}$$

Because the polarizability arising from an atomic transition is negative (positive) when an electric field is blue (red) detuned with respect to the respective resonance, there exist wavelengths between transitions for which $\alpha(\omega) \propto \Delta U = 0$. These *tune-out* wavelengths have utility for mixed-species traps and as precision test of QED [**TOforthcoming**, 37, 65]. During the course of my PhD research, I undertook a measurement of the the 413nm tune-out wavelength in helium under the leadership of B M Henson, and we achieved a 25x improvement over the last measurement. This measurement was the major motivation for acquiring the tunable laser described in the next chapter, and used to perform the experiments described in chapter **??**.

In heavier atoms than Hydrogen[9], interactions between electrons also play an important role, as we will see in the case of the most noble of metals and the central element of this thesis: Helium.

1.2 Helium

The idealized model of the hydrogen atom is fine for illustrating some important features of atomic physics, but the focus of this thesis is, of course, helium. Although the structure of the helium atom is simple enough that theoretical calculations can confidently accrue many significant figures, with precision rivalling similar calculations for Hydrogen, the presence of a second electron does considerably complicate the physics[10]. The Helium Hamiltonian

$$\left(\frac{-\hbar^2}{2m}\nabla_1^2 + \frac{-\hbar^2}{2m}\nabla_2^2 + \frac{e^2}{4\pi\epsilon_0}\left(-\frac{Z}{r_1} - \frac{Z}{r_2} + \frac{1}{r_{12}}\right)\right)|\psi\rangle = E|\psi\rangle$$

includes kinetic terms $\propto \nabla_i^2|\psi\rangle$ and a central potential $\propto 1/r$ for each electron, plus a repulsive interaction inversely proportional to the electron sepration r_{12}. The presence of a second electron also introduces another defining feature of quantum mechanics: spin. The electron wavefunctions must be antisymmetric under exchange of particle labels because all fermions obey the Pauli exclusion principle. On the other hand, the Hamiltonian is invariant under exchange of the electrons. If we denote the exchange operator by $\hat{X}$, then we have $[\hat{H}, \hat{X}] = 0$, implying $\hat{X}$ and $\hat{E}$ have the same eigenstates. Therefore the energy eigenbasis satisfies $\hat{X}|e\rangle = -|e\rangle$. Because the electron wavefunctions have the quantum numbers $|n, L, m_L, S, m_S\rangle$ which can be separated into the product of spatial ($|n, L, m_L\rangle$) and spin ($|S, m_S\rangle$) parts. It must be, then, that a given eigenstate must be of the form $|\psi\rangle = \psi^S_{space}\psi^A_{spin}$ or $\psi = \psi^A_{space}\psi^S_{spin}$

[9] Or as astronomers are wont to call them, 'metals'

[10] As the old joke goes, atomic physicists count '*one, two, many...*'

We can enumerate the possibilities for the symmetric (spin) wavefunctions,

$$\psi^S_{\text{spin}} = |\uparrow\uparrow\rangle, \tag{1.21}$$

$$|\downarrow\downarrow\rangle, \tag{1.22}$$

$$(|\uparrow\downarrow\rangle + |\downarrow\uparrow\rangle)/\sqrt{2} \tag{1.23}$$

and the antisymmetric term

$$\psi^A_{\text{spin}} = (|\uparrow\downarrow\rangle - |\downarrow\uparrow\rangle)/\sqrt{2}. \tag{1.24}$$

Which are all degenerate in energy because the atomic Hamiltonian does not couple to the spin sector. For a singly-excited helium atom, as will always be the case in this thesis, the interaction term splits the spatial part of the wavefunction for a given set of quantum numbers into symmetric and antisymmetric forms

$$\psi^A_{space} = \frac{1}{\sqrt{2}}\left(u_{1s}(1)u_{nl} - u_{1s}(2)u_{nl}(1)\right)$$

$$\psi^S_{space} = \frac{1}{\sqrt{2}}\left(u_{1s}(1)u_{nl} + u_{1s}(2)u_{nl}(1)\right)$$

which furnish the spin wavefunctions to form the n^3L_J and n^1L_J states, referred to as (triplet) ortho- and (singlet) para-helium, respectively[11]. It can be shown via degenerate perturbation theory that the exchange antisymmetry produces the *exchange energy* difference between the singlet and triplet states, where the orthohelium state has a lower energy. The 2^3S_1 state, also denoted He* , distinguishes helium amongst the zoo of atomic species available to the cold atom physicist by virtue of its 19.8 eV excitation energy and $\approx$ 7800s lifetime [41]. This state is forbidden to decay to the ground state by the $\delta L \neq 0$ selection rule and also because the dipole operator does not couple states of different spin, such as the He* state and $1s^2$ ground state. The state is therefore called *doubly forbidden*. Forbidden transitions can generally occur by higher-order interactions that are omitted from the dipole approximation, and the He* state in particular can decay via a magnetic dipole transition. Nonetheless, the two-hour lifetime is effectively a ground state for the purposes of ultracold helium experiments, which generally last less than a minute. Fortuitously, the metastable state is connected to the 2^3P_2 state by a transition with a wavelength of 1083.331nm, which is far more readily accessible with compact laser systems than the $\leq$ 63nm X-ray transitions from the true ground state. The 2^3P_2 state also provides a closed transition cycle for laser cooling as it can only decay to the He* state, obviating the need for an additional pump laser.

The astute reader will notice the absence of presentation of an explicit form for the electron wavefunctions in the helium atom. Indeed helium is not analytically solvable because its eigenfunctions not separable into a form $\Psi = \psi_1 \otimes \psi_2$. Furthermore, modern spectroscopy of helium has advanced to the level of accuracy where nuclear recoil effects must be included, which can be incorporated in the form of a series expansion in powers of $m_e/M_He \approx 10^{-4}$ Relativistic effects must be represented as another series expansion in powers of the fine structure constant $\alpha = \sqrt{2hcR_\infty/m_ec^2} \approx 1/137$. The combination of both corrections constitutes a double-series expansion of the form $\sum_i \sum_j \alpha^i (m_e/M_{He})^j$, and these terms can be calculated with sufficient accuracy to compete with modern experiments. A variational approach is required for tractable and accurate calculations, which was developed by Hylleraas [46, 45, 47]. In the intervening century, numerical methods for calculating the energy levels and transition rates in the Helium atom have kept pace with precision experiments, and a survey of recent progress is given in chapter **??**.

[11] In what follows, we use the spectroscopic convention and label states by the $n^{2S+1}L_J$, where $J = S + L$ because the helium nucleus is spinless, and we drop the $(1s)$ term as the second electron will invariably be in the ground state in all cases we consider - Doubly-excited helium is highly unstable because the first excited state (19.8eV) has about 80% of the ionization energy of Helium (25.4eV)

In real atoms, electrons are also bound by the laws of special relativity and interact with external fields and with the nucleus, which means the single-electron wavefunctions do not correspond perfectly to this form.

Magnetic fields and the Zeeman effect

The inclusion of spin introduces another important feature of atomic spectra, the Zeeman effect, whose discovery heralded a 'watershed' moment of modern physics[12]. The Zeeman effect refers to the phenomenon of spectral line splitting that occurs when an atom is immersed in a DC magnetic field, the synthesis of the prior concepts of the *normal* and *anomalous* Zeeman effect. The interaction energy of an atom in a magnetic field,

$$H = -\mu \cdot \mathbf{B}, \tag{1.25}$$

has contributions from both orbital and spin angular momenta ($\mathbf{L}$ and $\mathbf{S}$, respectively) through the atom's magnetic moment

$$\mu = -\mu_B \mathbf{L} - g_s \mu_B \mathbf{S}. \tag{1.26}$$

Working in the $|LSJm_J\rangle$ basis, where J and m_J are the total angular momentum and its z-projection, yields the eigenenergies $E_Z = g_J \mu_b B M_J$. The atomic g-factor can be written as

$$g_J = \frac{3}{2} + \frac{S(S+1) - L(L+1)}{2J(J+1)}, \tag{1.27}$$

using the approximate value of the electron g-factor $g_s = 2$.The eigenstates of the field-free atomic Hamiltonian will be $2J+1$-fold degenerate and specified by the $|Lm_L Sm_S\rangle$ quantum numbers. Adding the magnetic field interaction breaks this degeneracy and leads to the Zeeman splitting. The field-free and magnetic-interaction terms can be written in a common basis in terms of the Clebsch-Gordan coefficiencts and then diagonalized, as described in chapter **??**. The aforementioned anomalous Zeeman effect arises in triplet states because the inter-level spacing depends on m and g_J, which splits spectral lines as well as levels, whereas singlet states have $g_J = 1$ and transitions between them do not fan out in the same fashion. This distinction, whose explanation was an early victory for quantum mechanics, is illustrated in Figure **??**.

1.3 Interactions between atoms

For all the intricacy of atomic structure, life would be very dull indeed were it not for the interactions between them. Indeed, the material reality of the world depends, in a sense, less on the structure of its building blocks and more on how they fit together. The varied and central roles of interactions will be revisited in later chapters, but for now it will suffice to note that modern experimental techniques allow access to a large range of interaction strengths and modalities. For example, optical lattices or Feshbach resonances can be used to tune short-range interaction parameters between extreme values, from the ultradilute gases to the so-called strongly correlated regime. The spectrum of possibilities from isolated, to weakly-interacting, to distinctly many-body systems will be traversed over the course of the following chapters.

Here we briefly review elastic scattering, and then turn to important inelastic present in our experiments. An detailed primer in atomic scattering physics can be found in the classic texts [72] and [71], with more detail in the latter. An exhaustive review of low-temperature scattering studies up to the turn of the millenium can be found in [97]. I

[12] Along with the discoveries of X-rays, radioactivity, and the observation that 'cathode rays' had a mass-arge ratio equal to particles within atoms, now known as *electrons*[29]

focus here on two-body collisions, which are by far the dominant interactions in the low-density regime of ultracold gases. Low densities imply that low temperatures are required to achieve high phase space density and reach the degenerate regime. Two-body collisions are the crucial enabler for thermalization during the evaporative cooling necessary to reach such low temperatures, so long as the relaxation times are shorter than the sample lifetime, which is also determined by kinetic effects like three-body recombination or, in helium, Penning ionization.

Neglecting spin-orbit and relativistic effects the two-body scattering problem reduces to the Keplerian Schrödinger equation in the centre-of-momentum frame,

$$\left(\frac{\hbar^2}{2m^*}\Delta + V(r) - E\right)\psi(r) = 0, \tag{1.28}$$

in terms of the separation $r = |\mathbf{r}_1 - \mathbf{r}_2|$ between the particles and the reduced mass $m^* = m_1 m_2/(m_1 + m_2)$. In the asymptotic regime where r is much larger than the scale of $V(r)$, the solution takes the form of a superposition of the initial plane wave and the scattered solution,

$$\psi(r) \propto e^{ikz} + f(\theta)\frac{e^{ikr}}{r}, \tag{1.29}$$

where $k = \sqrt{2m^*E/\hbar}$ is the plane wave-vector of the initial approach and θ is the angle from the direction of incidence. A general solution can found by expanding $f(\theta)$ into a convenient basis of *partial waves* (spherical harmonics) which are labeled $s, p, d, f, ..$ in order of increasing angular momentum. In the low-energy limit, $f(\theta)$ is independent of angle and only the spherically symmetric s-wave term contributes, and the limit $f(\theta) \to -a$ is accordingly called the s-wave scattering length. At temperatures below 5mK the scattering physics is determined by just a few partial waves [62], and in the ultracold regime only the s-wave ~~matters~~ scattering channel is significant. The total cross section $|f(\theta)^2|/|\psi|^2$, which is the total probability that a near collision results in particle scattering, approaches $\sigma = 8\pi a^2$ for polarized bosons[13] [74].

The s-wave scattering length is also an important determinant of the energetics of degenerate matter such as BEC. Because BECs are dominated by long-wavelength behaviour, a theoretical treatement can be considerably simplified by considering only the *effective interactions*. By formulating the scattering problem in momentum space, the effective interaction strength for low-energy scattering $g = 4\pi\hbar^2 a/m$, also referred to as the pseudopotential, can be found by integrating out the high-frequency modes (also known as the Born approximation). This necessarily washes out extremely short-range correlations but makes fairly accurate calculations much more tractable, in particular those employing Hartree or Hartree-Fock methods. It is therefore difficult to overstate the importance of accurately knowing the s-wave scattering length for the purposes of understanding ultracold gas experiments.

In molecular collisions the scattering process will obviously depend on the relative orientation of the molecules. In collisions between single atoms, though, there is a more subtle orientation-dependence which arises from the total spin of the two-particle system. The three possible configurations between pairs of He^* atoms correspond to the singlet $^1\Sigma_g^+$, triplet $^3\Sigma_u^+$, and quintet $^5\Sigma_g^+$ Born-Oppenheimer molecular potentials, with total spin 0, 1, and 2[14]. When the atoms are spin-polarized, as they are when confined in magnetic traps, then the only scattering that occurs is in the quintet channel. The most accurate determination of the s-wave scattering length in this configuration is 7.512nm [66], in agreement with calculations performed the year before the measurements [74]. why is $a_{11} = a_{10}$?

[13] For fermion pairs with odd total spin, the cross section tends to zero because of the Pauli exclusion principle, and thus the s-wave scattering length vanishes.

[14] the subscript g and u are short for *gerade* and *ungerade* (German for even and odd) label the reflection symmetry of the two-body wavefunction, and the superscript + sign...

A powerful tool available in some cold atom experiments are Feshbach resonances[15]. A detailed description is found in [**Chin10**], but from an operational standpoint they allow control of the scattering length as $a = \tilde{a}(1 - \Delta/(B - B_0)$, where B is the strength of an ambient magnetic field, B_0 is the resonance value of the field, $\tilde{a}$ is the value when the field is far from a resonance and Δ sets the resonance width. The scattering length can thus be tuned in size and even in sign. Fundamentally, the stability of BEC requires a positive s-wave scattering length, and switching from stable to unstable configurations permits one to examine condensate collapse (as in the spectacular Bosenova experiments [**papers**]) and also to explore the BEC-BCS crossover [**papers**]. The spinless nucleus of ^{4}He prohibits coupling of bound states within an m_f manifold from crossing an open-channel threshold, precluding this pathway to a Feshbach resonance [31]. Nonetheless, Feshbach resonances induced by spin-spin interactions between helium atoms have been predicted [95, 31], but have not observed to date [12].

Inelastic scattering processes are those which exchange energy between the internal and motional states of either atom. They can be represented as a complex scattering potential [53] which permits losses from on-shell scattering channels. An important inelastic process characteristic of metastable noble gases [**VassenReview**] is *Penning ionization*. This can occur through the decay channels

$$\mathrm{He}^* + \mathrm{He}^* \rightarrow \begin{cases} \mathrm{He}^* \mathrm{He}^+ + e- & \text{(PI)} \\ \mathrm{He}_2^+ + e- & \text{(AI)} \end{cases} \tag{1.30}$$

Why is this spacing so huge? Formally, the first channel is called Penning ionization and the second is called Auto-ionization, but the rate of the latter is insignificant in comparison to the former [54]. Indeed, the energy of the metastable state is sufficient to ionize any neutral atom (except helium or neon) from its ground state, and [8] presents a tabulation of the ionization rates involving other species. Aside from attracting intensive study in its own right [**partridge10**, 87, 62], this explosive potential was a significant hurdle for researchers attempting to achive Bose-Einstein condensation with helium. The density achieved in early magneto-optical traps (MOTs) was limited to some hundredfold less than the alkali-metal MOTs of the day [**bardou92**, **kumukura92**, **mastwijk98**]. Helium MOT densities were limited by losses through two-body collisions involving atoms in the 2^3S_1 and those excited to the 2^3P_2 state by the trapping beams, as opposed to rescattering pressure as in the case of alkali metals. Such light-assisted collisions limited the density of helium MOTs and thus constrained their trapped population number until larger beams and detunings were used [93], whereby Penning ionization rates were reduced to the order of 5e-9 cm^3/s at large detunings, an improvement of about a factor of twenty. In the dark, the rate constant is a factor of 50 lower again, but the process is still too fast to permit access to magnetic traps of sufficient lifetime and density to reach degeneracy. Fortunately, the inelastic scattering cross-sections depend on the molecular potentials in such a way that condensation becomes attainable: When the atoms are polarized in the $m_J = \pm 1$ state, the collision takes place in the $^5\Sigma_g^+$ potential, while the reaction products have a total spin of 1, and so this process is forbidden. In reality, it does occur through a weak virtual spin-dipole transition [85] , but slowly enough that spin-polarized He* exhibits a 10^4-fold reduction in ionization rate. At field strengths above 50G, however, the suppression weakens [**Borbely12**]. Other noble gases also exhibit highly energetic metastable states, but the lifetime and suppressibility of Penning ionization decreases with increasing mass [67, 68]. Thus Helium may be the only noble gas ever to be Bose-condensed.

[15] Feshbach resonances originated in Feshbach's work in nuclear physics (Feshbach 1958, 1962) and Fano worked on in atomic context (fano 1961), but these fano-feshbach resonances are referred to in general as feshbach resonances.

1.4 Bose-Einstein condensation in dilute gases

The 'fifth state of matter'[16] has a long and storied history[2]. Following the oft-cited seven heroic decades between the initial theoretical descriptions and the experimental realization of atomic Bose-Einstein condensates [**anderson95**, 26, 79], the topic has become an industry in its own right at the eve of its centenary. As pithily put by a review only five years after the Nobel-winning experiments, 'Any attempt to review recent progress is out of date as soon as it is published' [16]. This is no less true today, as the number of ultracold gas experiments now number nearly 200[17] and numerous companies have been founded on the promise of selling better sensors and computers. Back in the middle of the 20th century, BEC garnered further attention when Fritz London proposed that Bose-Einstein condensation was connected to the superfluid phenomenon in liquid helium. Nikolay Nikolayevich Bogolyubov[18] formalized this connection and so, historically speaking, helium was the element which hosted the earliest experimental realization of Bose-Einstein condensation, albeit with a very small condensed fraction. While liquid helium is a rare thing in cosmological terms, BEC may have existed already for millions of years in the superdense dark matter of neutron stars [35, 61, 7, 69], wresting the claim of cosmic novelty from human hands. Nonetheless, the essentially pure atomic condensates and the emerging study of molecular condensates in laboratory settings are surely among the most extreme conditions in the universe. There are numerous treatments of the theory of Bose-Einstein condensation, for example the classic textbooks [72, 71] and review articles [18, 98, 16]. The essential background for discussed here draws on these standard sources unless otherwise cited.

The canonical description of Bose-Einstein condensation is the condition where the de Broglie wavelength associated with thermal kinetic energy

$$\lambda_T = \frac{h}{\sqrt{2\pi m k_B T}} \tag{1.31}$$

is comparable to the interparticle spacing, coinciding with a macroscopic occupation of the single-particle ground state as the de Broglie waves of many bosons constructively interfere. A precise criterion for this condition is when the phase space density

$$\aleph = n\lambda_T^3 \tag{1.32}$$

exceeds the critical value of $\zeta(3) \approx 2.612$. However, in the presence of interactions, this criterion is unsatisfactory: Just as interactions between electrons preclude an expression of the stationary states of helium in terms of products of single-particle energy eigenstates, the stationary states of an interacting gas of N atoms cannot be written as a prduct $|\Psi\rangle = |\psi_i\rangle^{\otimes N}$ of single-particle eigenstates $|\psi_i\rangle$. The Penrose-Onsager criterion [70] provides an alternative in terms of the density matrix ρ for the isolated composite system comprised of all the gas particles. The single-particle density matrix is then the expected value of the one-body field operator

$$\rho^{(1)} = \mathrm{Tr}\left(\rho \hat{\Psi}^\dagger \hat{\Psi}\right), \tag{1.33}$$

whose eigenvalues p_l^1 give the occupation probability of the l^{th} eigenvector of $\rho^{(1)}$. The eigenvectors themselves are the single-particle modes. If any eigenvalue p_l^i is proportional to N in the limit $N \to \infty$, then the system is said to have undergone Bose-Einstein condensation (or, simply, *condensed*) into the l^{th} mode.

[16] The familiar first phases, solid, liquid, and gas, are vanishingly rare in cosmological terms. The fourth, plasma, is the state of at leats 99% of the ordinary matter in the universe [1]. Helium compreses about 23%, most of which being primordial baryons formed during the recombination epoch.

[17] See `everycoldatom.com`

[18] Nikolay was a darling of Russian theoretical physics, receiving his PhD-equivalent qualification at 19 and made important contributions to quantum field theory. In his famous paper on the problem of interacting bosons, his name is transliterated as *Bogolubov*. Bogolyubov and *Bogoliubov* are also common transliterations.

Of course, real systems are subject to atom losses and heating, violating the assumptions of equlibrium underpinning both the approaches above. Nonetheless, the Penrose-Onsager criterion was found to be valid in a non-Hermitian polariton condensate [55]. Indeed, there are compelling reasons to call the experimentally realized ultracold gases 'Bose-Einstein condensates' without any qualms. As the saying goes, if it interferes like a condensate [5] , undergoes number fluctuations like a condensate [52], has HBT correlations like a condensate [80, 49], and quacks like a condensate [3], then it probably *is* a condensate.

While most atomic condensates, and all of those in this thesis, are trapped in non-uniform potentials, many important features of condensates are easier to state for homogeneous systems. One can usually extend calculations to harmonically trapped systems by a local density approximation, wherein one performs a density-weighted average across a condensate, considering each volume element as a homogenous condensate in its own right. Thus, for the most part the following discussion will focus on homogeneous systems for simplicity's sake. I present some particular results in the case of a harmonically trapped gas at the end of this section.

Bogoliubov theory

The fundamental theoretical object of interest is the Hamiltonian of a bosonic quantum field with two-body interactions,

$$\hat{H}\int\left(\frac{\hbar^2}{2m}\nabla\hat{\Psi}^\dagger(\mathbf{r})\nabla\hat{\Psi}(\mathbf{r})\right)d\mathbf{r}+\frac{1}{2}\int\left(\hat{\Psi}^\dagger(\mathbf{r}')\hat{\Psi}^\dagger(\mathbf{r})V(\mathbf{r}'-\mathbf{r})\hat{\Psi}(\mathbf{r}')\hat{\Psi}(\mathbf{r})\right)d\mathbf{r}'d\mathbf{r} \tag{1.34}$$

where $\Psi(r)$ are the field operators subject to the bosonic commutation relations

$$[\Psi(r),\Psi^\dagger(r')]=\delta(r-r') \tag{1.35}$$

$$[\Psi^\dagger(r),\Psi^\dagger(r')]=[\Psi(r),\Psi(r)]=0. \tag{1.36}$$

We can then write the field operator in the suggestive form

$$\hat{\Psi}=\psi_0\hat{a}_0+\sum_{i\neq 0}\psi_i\hat{a}_i \tag{1.37}$$

in terms of an orthonormal basis of single-particle modes ϕ_i and corresponding field operators $\hat{a}_i$. In doing so we distinguish $\mathbf{p}=0$ as the condensed mode, and say that condensation occurs when $N_0=\langle\hat{a}_0^\dagger\hat{a}_0\rangle\propto N$. The observation that the condensed mode has a population of order N means that in the thermodynamic limit ($N\to\infty$, $V\to\infty$), one particle here or there will not really make a measurable difference. This heuristic can be expressed quantitatively as the Bogoliubov approximation wherein the annihilation and creation operators for the condensed mode are replaced with complex numbers,

$$=\sqrt{N_0}e^{i\alpha},\hat{a}_0^\dagger=\sqrt{N_0}e^{-i\alpha}, \tag{1.38}$$

which permits the condensate wavefunction to take the form

$$\hat{\Psi}=\sqrt{N_0}e^{i\alpha}\psi_0+\delta\hat{\Psi} \tag{1.39}$$

$$=\Psi_0+\delta\hat{\Psi} \tag{1.40}$$

The first term is the condensate wavefunction, and the second corresponds to the population of non-condensed modes thanks to the effect of interactions, which are captured by the quasiparticle picture sketched in the next section.

The emergence of a condensate has many of the hallmarks of a classical phase transition: kinetic effects are necessary to redistribute energy and reach steady-state[19]; a unique critical

[19] Bose enhancement re: scattering into the ground state.

temperature T_c exists; below T_c an *order parameter* takes on a nonzero value; and condensation is equivalent to the spontaneous breaking of a U(1) gauge symmetry [99]. Above the critical temperature, $|\Psi_0| = 0$, and in general it exhibits a discontinuous derivative at the critical temperature. Hence, in the Landau-Ginzburg framework, condensation is a second-order phase transition[20]. The other hallmark of Landau-Ginzburg phase transitions is the spontaneous breaking of symmetry as one crosses ~~form~~ the disorderd to the ordered phase (as when a solid breaks the translational symmetry of the fluid phase). Condensates do exhibit such symmetry breaking: The Hamiltonian has a $U(1)$ gauge symmetry, but the ground state of a condensate spontaneously chooses a fixed but unpredictable phase α. By interfering two independently prepared condensates, one observes interference fringes [5], and indeed, the fringe locations will change with each realization and measurement. More directly, one can interfere light leakage from a reservoir-coupled photon condensate against a reference beam, and observe that phase jumps occur in the output when the condensate field drops to zero. That is, the re-emergence of the condensate is heralded by the selection of a new, specific, phase, apparently uncorrelated with the phase that existed before it [81].

Symmetry breaking is a subtle point discussed infrequently in standard textbooks. It happens that one can substitute complex numbers for the field operators, even when $\langle N_0 \rangle \to 0$ and still obtain correct results [30]: Condensation is not necessary for the Bogoliubov approximation to be valid. However, it *is* the case that the onset of condensation coincides with the ground state breaking the $U(1)$ symmetry [89] [21]. That this coincides with the validity of the 'coherent state' approximation is quite profound: Like the transition from the quantized electromagnetic field to the Maxwell equations, BEC has the flavour of a classical field but one which is consitued by matter which has dispersed in some delocalized state. The interactions between atoms present a marked departure from the physics of the electric field, however, and yet the system remains in the grasp of human theorists thanks to the Bogoliubov approximation, which I introduce here and examine experimentally in chapter **??**.

The Hamiltonian 1.34 has an alternative presentation in second-quantized form,

$$\hat{H} = \sum_{\mathbf{p}} \frac{p^2}{2m} a^\dagger_{\mathbf{p}} a_{\mathbf{p}} + \sum_{\mathbf{p},\mathbf{p},\mathbf{q}} \frac{\nu(\mathbf{p})}{V} a^\dagger_{\mathbf{p}+\mathbf{p}} a^\dagger_{\mathbf{q}-\mathbf{p}} a_{\mathbf{p}} a_{\mathbf{q}}, \tag{1.41}$$

where the $\hat{a}^\dagger_{\mathbf{p}}$ ($\hat{a}_{\mathbf{p}}$) operators create (annihilate) a bosonic atom in the state with momentum $\mathbf{p}$. The first sum is the kinetic term, and the second captures momentum-conserving collisions, where $\nu(\mathbf{p})$ is the Fourier transform of the scattering potential $V(\mathbf{r}' - \mathbf{r})$ and the sum omits terms which do not conserve momentum.

The Fourier conjugate of a contact interaction of the form $V(\mathbf{r}'-\mathbf{r}) = g\delta_{\mathbf{r},\mathbf{r}'}$ is $\nu(\mathbf{k}) = g/2$, which appears following a lengthy calculation (see, for example, [72]) in the symmetric quadratic form

$$H = \frac{gN^2}{2V} + \sum_{\mathbf{p}\neq 0} \frac{p^2}{2m} a^\dagger_{\mathbf{p}} a_{\mathbf{p}} + \frac{gn}{2} \sum_{\mathbf{p}\neq 0} \left(2a^\dagger_{\mathbf{p}} a_{\mathbf{p}} + a^\dagger_{\mathbf{p}} a^\dagger_{-\mathbf{p}} + a^\dagger_{-\mathbf{p}} a^\dagger_{\mathbf{p}} + \frac{mgn}{p^2} \right), \tag{1.42}$$

which is specified by $g = 4\pi\hbar^2 a/m$, and is visibly diagonalized in the non-interacting case, where $g = 0$. The off-diagonal scattering terms can be eliminated by following the Bogoliubov approach (which was actually first employed by Holstein and Primakoff in the context of spin waves [82] and then independently applied to the problem of interacting bosons by

[20] In the Ehrenfest picture one is instead concerned with the number of times one must differentiate some state function (e.g. specific heat, compressibility, pressure, free energy) before finding a discontinuity at the critical point. In this picture, the transition is first-order as one has continuous state functions with discontinuous derivatives.

[21] This is sometimes called 'breaking the gauge symmetry'. This is a misnomer, as a gauge symmetry is a property of the theory, not a state, and all consistent theories must be gauge symmetric throughout. These subtleties are discussed at length in lucid terms in [73]

Bogoliubov [**bologiubov47**]). The Bogoliubov transform amounts to the substitution of operators

$$a_{\mathbf{p}} = u_{\mathbf{p}}\hat{b}_{\mathbf{p}} + v_{\mathbf{p}}\hat{b}^{\dagger}_{-\mathbf{p}} \tag{1.43}$$

$$a^{\dagger}_{\mathbf{p}} = u_{\mathbf{p}}\hat{b}^{\dagger}_{\mathbf{p}} + v_{\mathbf{p}}\hat{b}_{-\mathbf{p}} \tag{1.44}$$

whose inverse

$$\hat{b}_{\mathbf{p}} = u_{\mathbf{p}}a_{\mathbf{p}} - v_{\mathbf{p}}a^{\dagger}_{-\mathbf{p}} \tag{1.45}$$

$$\hat{b}^{\dagger}_{\mathbf{p}} = u_{\mathbf{p}}a^{\dagger}_{\mathbf{p}} - v_{\mathbf{p}}a_{-\mathbf{p}} \tag{1.46}$$

make clear their physical interpretation: the $\hat{b_{\mathbf{p}}}$ operators act on the subspaces corresponding to *collective excitations* which are made up of superpositions of oppositely-moving single particles. This correspondence has been directly observed in experiments [96] using absorption imaging techniques; an unrealized goal in cold-atom science is the observation of this single-particle decomposition at the level of single atoms. More will be said about the challenges of this goal in chapter Y.

The quasiparticles are pairs of bosons, whose total spin will also be an integer, and thus the $\hat{b}$ should obey the bosonic commutatation relations. This constrains the coefficients such that $|u_{\mathbf{p}}|^2 - |v_{-\mathbf{p}}|^2 = 1$, permitting the parametrization $u_{\mathbf{p}} = \cosh\alpha_{\mathbf{p}}$, $v_{-\mathbf{p}} = \sinh\alpha_{\mathbf{p}}$. One picks $\alpha_{\mathbf{p}}$ such that the off-diagonal terms in the transformed Hamiltonian vanish, which provides the form

$$u_{\mathbf{p}}, v_{-\mathbf{p}} = \pm\sqrt{\frac{p^2/2m + gn}{2\epsilon(p)} \pm \frac{1}{2}}, \tag{1.47}$$

in terms of the Bogoliubov dispersion relation

$$\epsilon(p) = \sqrt{\frac{gn}{m}p^2 + \left(\frac{p^2}{2m}\right)^2}. \tag{1.48}$$

One could rewrite $\epsilon(p)$ in terms of the speed of sound $c = \sqrt{gn/m}$ to obtain the alternative form $\epsilon(p) = \sqrt{p^2c^2 + \left(\frac{p^2}{2m}\right)^2}$, making clear the extreme behaviours of the excitations: At low momentum, they are wavelike phonons with $\epsilon \approx pc$ and at high momentum they are effectively free particles with $\epsilon \approx p^2/2m$, with the smooth intermediate region determined by the effective coupling strength g.

The population of the single-particle states can be calculated by substituting the quasiparticle field operators into the standard expectation value, giving

$$n(\mathbf{p}) = \langle\hat{a}^{\dagger}_{\mathbf{p}}\hat{a}_{\mathbf{p}}\rangle \tag{1.49}$$

$$= \langle\Psi|(u_{\mathbf{p}}\hat{b}^{\dagger}_{\mathbf{p}} + v_{\mathbf{p}}\hat{b}_{-\mathbf{p}})(u_{\mathbf{p}}\hat{b}_{\mathbf{p}} + v_{\mathbf{p}}\hat{b}^{\dagger}_{-\mathbf{p}})|\Psi\rangle \tag{1.50}$$

$$= \langle\Psi|(u^2_{\mathbf{p}}\hat{b}^{\dagger}_{\mathbf{p}}\hat{b}_{\mathbf{p}} + v^2_{\mathbf{p}}\hat{b}_{-\mathbf{p}}\hat{b}^{\dagger}_{-\mathbf{p}} + u_{\mathbf{p}}v_{\mathbf{p}}\left(\hat{b}_{-\mathbf{p}}\hat{b}_{\mathbf{p}} + \hat{b}^{\dagger}_{\mathbf{p}}\hat{b}^{\dagger}_{-\mathbf{p}}\right))|\Psi\rangle. \tag{1.51}$$

In the steady-state, the expected value of the mode populations is constant and hence the third term is zero because it does not conserve particle number. It follows from the bosonic commutation relations that

$$\langle\Psi|\hat{b}_{-\mathbf{p}}\hat{b}^{\dagger}_{-\mathbf{p}}|\Psi\rangle = \langle\Psi|1 + \hat{b}^{\dagger}_{\mathbf{p}}\hat{b}_{\mathbf{p}}|\Psi\rangle \tag{1.52}$$

$$= \langle\Psi|\Psi\rangle + \langle\Psi|\hat{b}^{\dagger}\hat{b}|\Psi\rangle \tag{1.53}$$

hence the second term survives and allows the population to be written as

$$n(\mathbf{p}) = (u^2_{\mathbf{p}} + v^2_{\mathbf{p}})\langle\hat{b}_{\mathbf{p}}\,\dagger\,\hat{b}_{\mathbf{p}}\rangle + v^2_{\mathbf{p}}, \tag{1.54}$$

Where the quasiparticle population can be computed from the Bose-Einstein statistics as

$$\langle \hat{b}^\dagger_{\mathbf{p}} \hat{b}_{\mathbf{p}} \rangle = \frac{1}{e^{\beta\epsilon(p)} - 1}, \tag{1.55}$$

and the corresponding population of $\mathbf{p} \neq 0$ single-particle modes is the thermal population. The $v^2_{\mathbf{p}}$ term persists even at $T = 0$ and, owing to its nature as the zero-point energy of the quasiparticle vacuum, gives rise to a population outside the condensed mode known as the *quantum depletion*, which is the focus of chapter Y.

Harmonically trapped condensates

Turning back toward harmonic gases, we can begin from the full Hamiltonian (Eqn. (1.34) and produce an effective Schrödinger equation, by assuming slow variations in the density, integrating out short-wavelength modes as in the Born approximation and arriving at the Gross-Pitaevskii equation (GPE),

$$-\hbar\partial_t \Psi(r,t) = \left(-\frac{\hbar^2\nabla^2}{2m} + V(r,t) + g|\Psi(r,t)|^2 \right) \Psi(r,t). \tag{1.56}$$

which is valid for arbitary interactions dominated by the s-wave scattering length. If one further assumes that the condensate density varies on scales larger than the healing length $\xi = \hbar/\sqrt{2mgn}$, one can make the Thomas-Fermi approximation and ignore the kinetic term in the GPE, whereby the condensate density profile can be written as

$$n(\mathbf{r}) = \frac{\mu - V(\mathbf{r})}{g}, \tag{1.57}$$

where μ is the chemical potential. For a Bose gas confined in a harmonic potential of the form

$$V = \frac{1}{2}m\omega_x^2 x^2 + \frac{1}{2}m\omega_y^2 y^2 + \frac{1}{2}m\omega_z^2 z^2, \tag{1.58}$$

this produces the famous inverted-parabola density profile, for which the peak density of the condensate is

$$n_0 = \frac{1}{8\pi}\left((15N_0)^2 \left(\frac{m\bar{\omega}}{\sqrt{a_{1,1}}\hbar} \right)^6 \right)^{1/5}. \tag{1.59}$$

The Thomas-Fermi approximation ~~which~~ is valid when $Na/a_{ho} \gg 1$, where $a_{ho} = \sqrt{\hbar/m\omega}$ is the length scale of the ground state of the harmonic oscillator. The phase space density for condensation is achieved at the (ideal) critical temperature

$$T_c^0 = \frac{\hbar\bar{\omega}}{k_B}\left(\frac{N}{\zeta(3)} \right)^{1/3} \tag{1.60}$$

$$\approx 0.94\frac{\hbar\bar{\omega}N^{1/3}}{k_B}. \tag{1.61}$$

where $\bar{\omega} = (\omega_x\omega_y\omega_z)^{1/3}$ is the geometric mean of the trapping frequencies. The condensed fraction below the critical temperature is

$$\frac{N_0}{N} = 1 - \left(\frac{T}{T_c^0} \right)^3, \tag{1.62}$$

Interactions between particles reduce the critical temperature in a harmonic trap, and the resulting shift in the critical temperature can be written as

$$\frac{\delta T_c}{T_c^0} = -1.3\frac{a}{a_{ho}}N^{1/6} - 0.73\frac{\langle\omega\rangle}{\omega_{ho}N^{1/3}} \tag{1.63}$$

where the latter term, the correction for finite atom number, includes the arithmetic mean trapping frequency $\langle\omega\rangle$ and vanishes in the thermodynamic limit ($N \to \infty$, $V \to \infty$, N/V finite). This effect can be understood in terms of the reduction in density due to repulsive interactions, thus driving down the phase space density $n\lambda^3$ at a given temperature, lowering the temperature required for condensation. These deviations from ideal behaviour have been observed in experiments [91, 86].

The condition $\mu - V(\mathbf{r}) = 0$ determines the boundary of the condensate, giving the Thomas-Fermi radii $R_i = \sqrt{2\mu/m\omega_i^2}$, where $i \in \{x, y, z\}$. The chemical potential for the harmonically trapped condensate also fixes the average energy per particle:

$$\mu = \frac{\hbar\bar{\omega}}{2}\left(\frac{15Na}{a_{ho}}\right)^{2/5} = \frac{7}{5}\frac{E}{N} \tag{1.64}$$

As for the practical production of condensates, much quality literature has been written on the theory and techniques of atomic cooling technqiques employed to reach degeneracy. These days, such techniques are standard across hundreds of laboratories and so space will not be spared for their general consideration here. The curious reader is directed to [**courtielle01**, **tychkovThesis**, 50, 63] for detailed discussions. Rather, ~~for~~ in the next chapter, I discuss the specifications of the apparatus used in the course of this research to implement the general principles of atomic cooling and trapping to achieve condensation.

Chapter 2

Experimental infrastructure

"Every sensor is a temperature sensor. Some sensors measure other things too."
- Engineer's aphorism[1]

This dissertation spans works conducted on two experimental apparatus. The major works discussed in chapters **??** and **??** were undertaken on an existing machine, which has been in productive operation for many years. This machine achieved BEC in 2007 [24], utilizing a bright cold beam of helium [90] and optimized Zeeman slower [28]. Key technical facilitations were the installation of auxiliary field coils for active cancllation of stray magnetic fields [28] and temperature control at the centikelvin level at the BEC chamber[2] by control of the cooling air mixture [27]. The machine has had a storied history since then, hosting a range of experimental themes including many-body correlations [43, 21, 56] (especially Hanbury Brown-Twiss correlations [58, 25, 39, 77, 78]), studies of atom lasers [24, 19, 36, 58] and guided matter waves [23, 25, 22], and quantum-optics demonstrations such as single-particle sources [57], ghost-imaging [51, 40], Wheeler's delayed choice thought experiment [60], and bell-type correlations between pairs of freely propagating atoms [84] (as well as their utility for magnetometry [83]). This apparatus has been employed for laser spectroscopic studies of helium structure including the 413nm tune-out wavelength (as first reported in [37] and improved during the course of this thesis, with publication forthcoming) and transition energies [76, 92]. This machine is described in great detail in past publications (in particular [90, 24]) and PhD dissertations [**hodgmanthesis**, **manningthesis**, **shinthesis**, **dallthesis**]. In this section, therefore, the apparatus will be summarily described, and the motivated reader referred to the aforementioned sources for more information. Given the maturity and ubiquity of atom cooling and trapping techniques, cursory descriptions of the important experimental stages are provided. For more details the reader is referred to the texts [29, 63] and prior dissertations [**hodgmanthesis**, **manningthesis**, **dallthesis**].

About half the duration of this course of study was devoted to the refurbishment of a retired cold-atom experiment towards loading a He^* BEC into an optical lattice. Before its erstwhile retirement, this machine was used for the study of electron scattering and dual-species MOT experiments[94, 14, 15], and determination of electronic transition rates [20, 41, 42] in He^* . The renovation of this machine was motived by the insufficient optical access into the BEC chamber of the already-operating machine, preventing a straightforward upgrade. These machines can be distinguished between these two by their intended final trapping method: The machine discussed in the previous paragraph could therefore labelled the *BiQUIC machine*, and the upgraded apparatus referred to as the *lattice machine*. In an attempt to convey their unique personality, I assign, and occasionally use, the nicknames *cacophanous harmony* and *staggering grace*, respectively. BEC was recently achieved in the Staggering Grace by the resident graduate students [4], and the construction is ongoing. As

[1] Quoted without attribution in Elecia White's *Making Embedded Systems*, O'Reilly media, 2011
[2] also known affectionately as the *science chamber*.

Staggering Grace has yet to produce scientific results in its newfound youth, I will discuss the scientific motivation for its construction and my contributions to the project in chapter **??**. This chapter is concerned with the anatomy of the first machine, which hosted the works described in chapters **??** and **??**. The distinctive features of the refurbished machine will be described in chapter **??**.

2.1 Helium beamline

In brief, both BEC machines exist to achieve magnetic trapping of metastable helium in ultra-high vacuum (UHV) conditions [3]. Magnetic trapping is required because the limits of optical cooling are too hot to achieve degeneracy with the conventional densities. Optical cooling techniques are required to achieve low enough temperatures such that the magnetic trap can be filled with a suitable population to reach BEC by evaporative cooling. The pecularities of producing He^* atoms and the need for multiple optical interfaces into UHV conditions demand large devices with many hundreds of moving parts.

The fundamental minimum for laser cooling by radiation pressure is the *recoil limit* set by the relation $k_B T = \hbar^2 k^2 / 2m$, where k is the wavevector of the cooling light. This is the energy scale fixed by a single-photon emission, and is about 2 μK for Helium. While this is too hot to achieve condensation in the traps considered in this thesis (whose critical temperature is about 1 μK), we generally only use laser cooling down to the *Doppler limit*. The latter is given by $T = \hbar\Gamma / 2k_B \approx 38$ μK and corresponds to the minimum velocity difference which can be distinguished by the cooling laser. In practise this is set by the linewidth Γ of the cooling transition, as the laser linewidth is smaller by about an order of magnitude[**shin16**]. These limits of optical cooling mean that laser cooling of helium to the ground state of our traps is not possible. Furthermore, helium has a spinless nucleus and thus no hyperfine structure, precluding the polarization-gradient cooling employed in alkali atoms. Fortunately, condensation is achievable in magnetic traps. The pathway from room temperature to degeneracy is outlined in the rest of this section.

He^* atom source

The metastable He^* state is generally produced by an electric discharge as opposed to optical excitation due to the lack of convenient X-ray light sources at 63nm. Electons accelerated by a strong potential gradient can ionize helium atoms, and thus also have enough energy to excite atoms into the He^* state. In our experiments, a grounded copper block cooled by liquid nitrogen serves as the anode and reaction vessel. A tungsten cathode is held at 2kV and placed in front of the vessel, separated by insulating ~~maycor~~ spacers. The source is ignited at a higher pressure than normal operation, because the breakdown voltage of helium gas in this geometry is too high at typical operating pressure, which is optimized for loading a large population in the second MOT. The Paschen curve for helium is minimized at a slightly higher pressure, but even at this point an additional 500V boost is required to ~~reach~~ overcome the minimum breakdown voltage achieve ignition. Unfortunately, the DC discharge only excites about .01% of the atoms into the He^* state [87], and multiple collisions impart fairly high velocities to the light helium atoms, despite being cooled by liquid nitrogen. This necessitates a larger Zeeman slower stage than is found in other cold-atom apparatus.

The source chamber tends to operate consistently over several months, permitting development and execution of a handful of experimental campaigns. However, the copper housing can degrade with time, causing intermittent source extinctions or even preventing successful striking altogether. This is usually remedied by extracting the source chamber from the vacuum system and skimming a few microns of copper from the interior surface of the block. This procesure is generally straightforward but somewhat painstaking.

[3] Sometimes called *hard* vacuum. Both terms are amusingly paradoxical.

Beam forming

The gas expands out of the forward-facing aperture of the reaction vessel and a small solid angle is selected by a skimming nozzle between the source chamber and the rest of the helium beamline. The skimmer serves a secondary purpose as a weak differential pumping stage, keeping the first laser cooling stages at a lower pressure than the source chamber. The beam is collimated[4] by a single beam reflected in a figure-4 configuration, forming a a 2D optical molasses[**Lett81**, **rooijakkers96**] and providing cooling in the two transverse degrees of freedom. This is followed by a 'bending' stage wherein a resonant single beam deflects the metastable atoms by a few degrees through a second stage of differential pumping into the Zeeman slower chamber. This provides better selectivity of He^* atoms by reducing the number of unexcited atoms that enter the Zeeman slower and first MOT chambers.

Zeeman slowers, so named for the exploitation of the Zeeman effect, are necessary to slow atoms from thermal velocities imparted from their sources to below the capture velocity of the magneto-optical traps located at the end of the slower. The Zeeman slower in our experiment [28] reduces the most probable longitudinal velocity of the beam from $\approx$ 700 m/s to $\approx$ 70 m/s, which permits loading of the MOT to a steady-state population in about one second.

First Magneto-Optical Trap

The magneto-optical trap combines the radiation pressure with a spatially-varying magnetic field. When atoms move away from the centre of the trap, a restoring force is created as the atoms move into resonance with a counterpropagating laser beam. A quadrupole magnetic field ensures atoms are resonant as they approach an ellipsoid surrounding the trap centre, thus confining atoms within the trapping area. This technique was first proposed by Jean Dalibard and eventually realized by Raab *et al* [**raab87**]. Early helium MOTs were limited in number because of the size of the trap. Later attempts achieved larger number by operating with larger beams and detunings (-22Γ), obtaining lower densities than in other species [93] and mitigating losses due to Penning ionization. The multifaceted physics of MOTs has proven rich ground for study in general [**Townsend95**, **walker90**], and also in the specific case of helium, for which the two-body loss rate has been studied [93] along with the roles of light-assisted collisions [**papers**]. Temperatures in a MOT are, at best, on the order of the steady-state molasses temperature $\approx$ 1 mK [**Lett81**]. Further evaporative cooling is therefore required to reach quantum degeneracy. The background pressure in the first MOT chamber is still too high to maintain a long-lived magnetic trap. Therefore, the first MOT is used as a source for a secondary helium beam which feeds into the final science chamber. The MOT chamber features a $\approx$2mm hole bored through a compound quarter-waveplate-and-mirror mounted at the back of the vacuum chamber, which adjoins the transfer conduit supplying the BEC chamber with cold helium.

A slightly blue-detuned 'push' beam is ~~roughly~~ aligned with the aperture at the back of the first MOT to transfer atoms into the second MOT along ballistic trajectories [90]. In practise the beam points slightly upward, and the orientation is optimized by maximizing the saturated fluorescence signal in the second MOT. The atoms pass through a 'focus' stage consisting of two crossed, retro-reflected laser beams with a $\approx$1cm waist. Wire coils mounted around the 3/4" window flanges create an octupole magnetic field surrounding the beamline such that the circularly-polarized beams address only atoms on the proximal half of the beam to the optical insertion. This provides a final stage of transverse cooling and increases the interaction strength between the beam and the second MOT, in turn increasing the capture efficiency. The focusing stage typically increases the saturated fluorescence signal in the second MOT by at least 50%.

[4] Technically speaking, the beam is not collimated in the same manner as a laser beam. The divergence is reduced, but not enough for the beam to converge to a focus further along the beamline. Similarly, the 'focus' stage described below does not create a convergence but provides additional transverse cooling.

The Science Chamber

The second trapping chamber is evacuated to a pressure of some 10^{-11} mbar, which provides an excellent magnetic trap lifetime of several minutes. The chamber is surrounded by three pairs of square magnetic coils which actuate active cancellation of stray fields from the earth and nearby electronic equipment[5] [**dedman07**]. This assists the creation of a stable magnetic trap with two coil pairs in a Bi-planar quadrupole Ioffe configuration (BiQUIC) [24]. Magnetic traps exploit the interaction of the atomic magnetic dipole with a magnetic field, which takes the form $E_B = -\mu \cdot \mathbf{B} = -\hbar g m_J B$, where g is the atomic g-factor and m_J is the projection of the total angular momentum onto the magnetic field vector. A magnetic field with a local extremum can therefore form a confining potential for the states whose energy is minimized at this point. It follows from the Maxwell equations that a magnetic field in free space cannot have any local maxima [50], and so one must select an atomic state with $gm_J > 0$ for confinement at a local minimum of the magnetic field. In He* this uniquely selects the $m_J = +1$ state for magnetic trapping, which also ensures complete spin-polarization and the attendant reduction in Penning losses. The BiQUIC design is a solution to a critical issue with early traps [**migdall85**]: The quadrupole fields generated by coils in an anti-Helmholtz configuration feature a zero crossing in the trap centre. Atoms in a magnetic field undergo transitions to untrapped states, known as *Majorana transitions*, at a rate proportional to $\exp(-B/\omega)$, where ω is the trapping frequency and B is the magnitude of a (uniform) magnetic field [88]. In harmonic traps the trap bottom thus sets the upper bound on the Majorana transition rate [13]. Many variations on the quadrupole trap exist to mitigate this issue, including the Time-Orbiting Potential (TOP) [**TOPPaper**], Ioffe-Pritchard [**pritchard83**], cloverleaf [64], and QUIC [**esslinger98**] traps. Other groups have added a repulsive dipole potential to the trap zero with a focused and blue-detuned laser beam [**papers**].

In addition, a pair of low-intensity Doppler cooling beams are inserted at 15° relative to the horizontal. A vacuum window on the opposite side to the helium beam provides optical access for a spectroscopic probe beam or the 1550nm beams used for atom-optics techniques (employed in works not relevant to this thesis). The final optical component is a diagnostic photodiode mounted outside the chamber and is used to measure a saturated fluorescence signal, which serves as a diagnostic for the in-trap population. Two radio coils, including one in-vacuum coil and a second antenna inserted into one of the coils of the BiQUIC trap, provide the radio signals for the evaporative cooling and atom lasers, respectively. The evaporative cooling ramp is generated by an arbitrary waveform generator pre-loaded with a time-varying frequency ramp ~~by~~ created with the LabView control software (see below). The secondary coil is driven by a function generator, and both signals are passed through a dedicated 30W amplifier before insertion into the chamber.

Optimizing machine performance

Routine maintenance is required to keep the machine capable of producing large condensates. Despite the stabilized environment, optics are prone to wander slightly over time. The stable temperature is especially important as the cooling beams are coupled from the AOM tables to the vacuum chamber optics by free-space links. Drift in the relative position of the optics tables would therefore result in misalignment of many laser beams, and degrade performance of the machine. The conditioned air is supplied through three HEPA filters in the lab ceiling. The resulting positive pressure in an area enclosed by PVC strip walls keeps dust from entering the area on air currents.

If the second MOT is loading and a saturated fluorescence signal is visible, one can usually optimize all of the optical alignments on this signal, which is a factor of ten faster

[5] The 'nuller' reduces, but does not eliminate, 50Hz noise from the AC mains supply to the laboratory. We also measured a sub-percent level change in the trapping frequency when a metal chair was placed near the science chamber during an alignment effort.

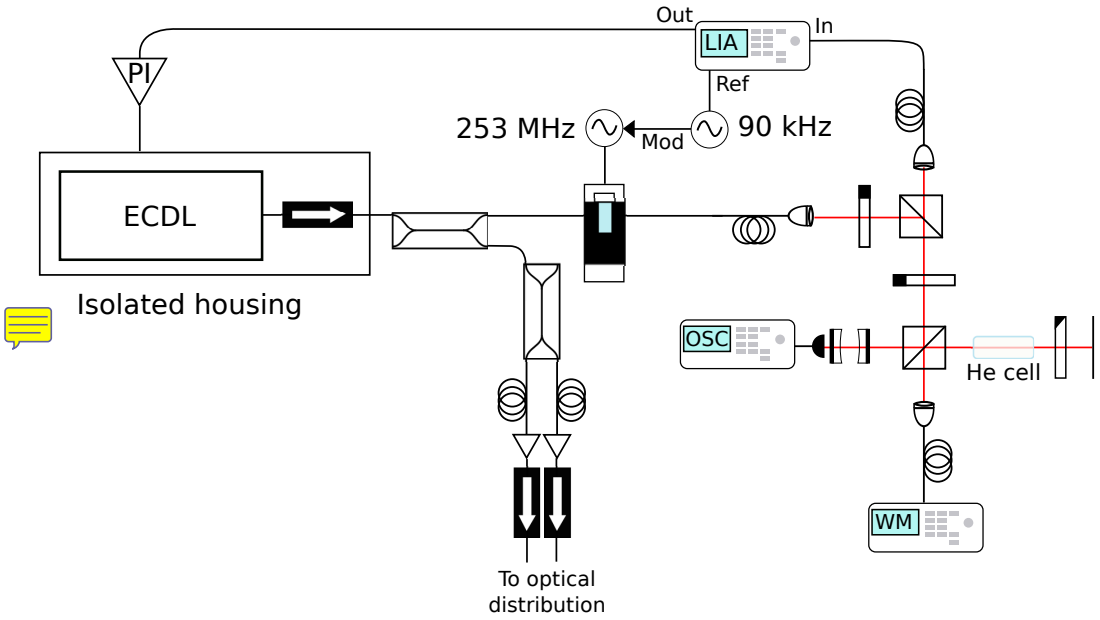

Figure 2.1: Schematic of the generation and control system for the main cooling laser operating at 1083.331nm. double check unused channel

than the full BEC creation sequence. If this is not available, historical records of diagnostics taken at several points throughout the beamline can facilitate diagnosis of the point of failure. The most commonly employed tests are faraday cups which produce a current when impacted by He^* atoms, as read out on a picoammeter. These current sensors are placed after the deflection stage, at the end of the Zeeman slower (with a large hole bored through it to allow the slowing beam to pass through), between the first MOT and the focus stage, and behind the second MOT chamber. In case the first MOT is not operational, a Xenics Bobcat CCD camera mounted above the chamber provides a view of the trapping region and direct visual feedback about the presence, shape, and density of the MOT.

2.2 Light sources

The principal light source for both experimental apparatus is the 1083nm cooling and trapping laser. The light source is an external-cavity diode laser which is depicted in Figure 2.1, published in [**shin16**] and detailed in the PhD thesis of D. K. Shin [**ShinThesis**]. The laser output passes through an in-fibre beamsplitter, of which one output is blue-shifted by 253MHz by an acousto-optical modulator (AOM) and locked to a helium gas cell by saturation absorption spectroscopy. The remaining arm is coupled by optical fibres to the fibre amplifiers of both experiments. The supply of light which is 253MHz red of the field-free resonance reduces the risk of stray light interacting with atoms and disrupting the delicate cooling and trapping processes. Each experiment features its own fibre amplifier that produces ≈ 3 W of laser power from the ≈ 100 μW supplied by the ECDL.

Both machines also employ sources of 1550nm laser light, used for a crossed optical dipole trap in the lattice machine, and to implement atom-optical control elements in the BiQUIC machine. The latter techniques are mentioned here for completeness but are not discussed further as they were not used in the works in this thesis. The construction and operation of the 1550nm optics for the lattice machine are described in chapter **??**.

Optical distribution setups

In each machine, a suite of AOMs are used to independently control the power and frequency of each of several specialized beams [6]. The first-order diffraction is usually chosen for its more efficient transmission. The pointing of the diffracted beams vary with the AOM frequency, which is a problem when the ultimate destination of the light is separated from the AOM by several meters of optical path length, after which the deflection can become significant. To circumvent this, the AOMs are set up in a double-pass 'cat's-eye' configuration so the deflection in one pass is canceled by the second pass in the opposite direction.

The AOM suites are supplied by light picked off from the output of the fibre amplifier by a half-waveplate and beamsplitter pair per AOM, as depicted in 2.2[7]. A quarter-wave plate placed in the optical path through the cat's-eye ensures the doubly-diffracted beams are transmitted back through the beamsplitter into the distribution optics. AOMs offer the advantage of fast switching times, but some light can leak from the AOM suite through the optical paths into the experiment. As such we used electronic shutters and an opaque enclosure to prevent this from occurring. The shutter action as well as the detuning and diffraction efficiency of the AOMs are actuated by the control software described later in this chapter.

Spectroscopic laser

A light source unique to the BiQUIC machine was the tunable laser system used to generate light in the $402 - 430$nm range for the laser spectroscopy measurements discussed in Chapter **??**. This was a tunable M-squared Ti:Sapphire laser system, depicted in Figure 2.3. Light at 1064nm from a Lighthouse Photonics Sprout module was frequency doubled by second-harmonic generation to pump an M-squared SolsTi:S titanium-sapphire laser which we operated around 800nm. The output from the SolsTi:S was doubled again in an M-squared ECD-X module to the target wavelengths. A fraction of the light is fed into a High Finesse WS-8 wavemeter. High Finesse specifies the absolute accuracy of the WS-8 at 2MHz within 2nm of a transition line, and 10MHz otherwise. We use the wavemeter to lock the tunable laser with respect to the red light, so the uncertainty is doubled in determinations of the blue frequency. We calibrated the wavemeter once every day or so with respect to the two-photon crossover transition between the $6^2P_{\frac{3}{2}}(F = 4)$ and $6^2P_{\frac{3}{2}}(F = 5)$ lines in a cesium vapor cell. We used saturated absorption spectroscopy to lock the red light to the Cs transition while feeding light into the wavemeter for the calibration. A MATLAB software lock uses the wavemeter output to stabilize the laser to within 100kHz of the target wavelength, and allows atomatic scans across the region of interest by automatically updating the laser set point. description of TCP lock protocol

We used the first diffracted mode of an AOM, driven at 189MHz, to control the beam power. The output of the AOM was fed into an optical fibre which coupled the light to the vacuum insertion optics. There, we used waveplates to set the polarization and a telescope to magnify the beam up to ≈2cm waist. A final lens fixed to a three-axis translation mount was used to focus and align the beam. For the measurements of the tune-out and forbidden transition wavelengths, we focused the beam to a diffraction-limited waist, about 100 μm at the site of the BEC, to achieve strong interaction given the weak signals of interest. For the $2^3P_2 \rightarrow 5^3D$ transitions described in the bulk of Chapter **??**, the beam was collimated and operated at a reduced power to mitigate power broadening and saturation of these much

[6] The active component of an AOM is a crystal is driven at radio frequencies by an amplified voltage-controlled oscillator. An acoustic standing wave, constituted by phonons with frequency matched to the driving frequency, scatters light into discrete diffraction modes width momenta shifted by the phonon-lattice momentum. The action is analogoous to a diffraction grating, and described by the Kapitza-Dirac mechanism. Thus the AOM transduces electronic signals into optical frequency shifts. An analogous effect, with the role of atoms and light interchanged, is the operating principle of optical lattices.

[7] This figure shows the AOM suite layout for the lattice machine, as I built it when working on the project. The layout for the BiQUIC machine is essentially the same.

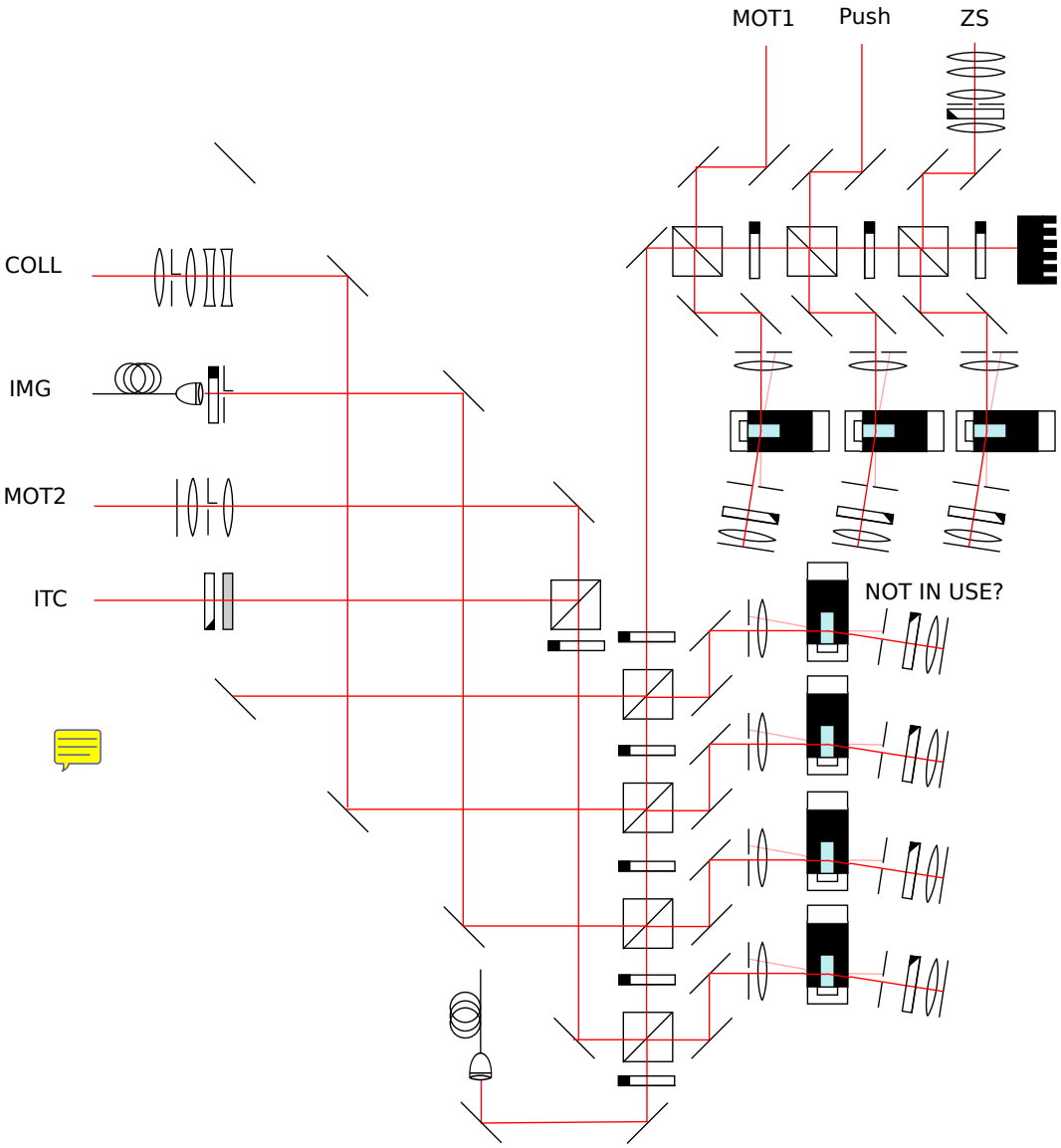

Figure 2.2: Schematic of the control and distribution system for cooling light in the lattice machine.

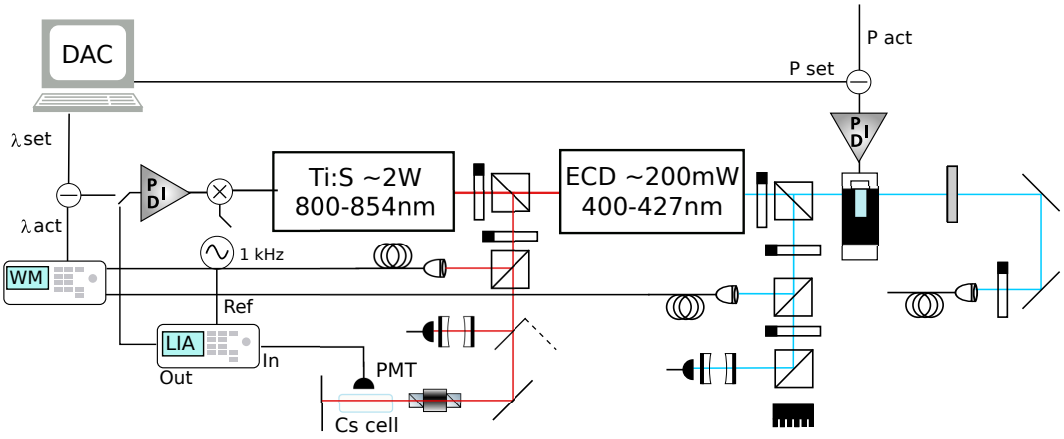

Figure 2.3: Schematic of the spectroscopic laser system, including calibration infrastructure.

stronger resonances. The optical power was regulated with reference to a photodiode which sampled the beam after the fibre via a polarizing beamsplitter.

The wavemeter logs, photodiode voltage, and transmission of light from both the 800nm and 400nm beams through two scanning Fabry-Perot cavities (SFPs) were recorded through the DAC system in order to provide diagnostics in post-processing. Part of the data analysis pipeline then automatically discarded shots where either SFP showed multiple peaks within a single free-spectral range (FSR), indicating that one of the lasers was running in a multimode regime, or where the photodiode trace indicated a laser supply failure, or where other anomalous behaviour was detected.

MATLAB lock loop

2.3 Detection of metastable helium atoms

A unique diagnostic available in helium experiments is the production of helium ion-electron pairs. This process can be monitored by in-vacuum electron multipliers mounted near the trapping region. Proximity to the trap is desirable for efficient collection of the resulting particles. Aside from investing Penning ionization itself (as mentioned earlier in this chapter), ion detection has been applied in photoassociation spectroscopy [38, 48], to monitor the onset of Bose-Einstein condensation [**tychkov06**], and for high-precision laser spectroscopy [75]. The ion detector in Cacophanous Harmony stopped working some years ago and has not been replaced: the utility of this diagnostic is outweighed by the effort required to break vacuum for the first time in a decade or so, disassemble the chamber and surrounding optics, reassemble everything, bake the chamber, and realign all the optics. As such ion detection garners only a brief mention in section **??**, wherein I describe an attempt to use the ion detection as an diagnostic to aid alignment of a dipole beam in the lattice machine. In an accident a year or so after I left that lab, the ceramic feed-throughs connecting the ion detector to the external electronics cracked. This broke vacuum, necessitating a rebake of the chamber, and saw the detector retired.

Two optical detection methods are employed in the ANU helium labs. Saturated fluorescence measurements are used to monitor the number of atoms in a trap. In this method, bright resonant light ($I \gg I_{\text{sat}}$) is applied to the atoms such that the population of the excited state saturates at 50%. If the light is applied while the trap remains on, then while some atoms may decay to a trapped state, repeated absorption events eventually drive them out of the trap. Therefore, one expect a sharp peak and subsequent decay in the optical power re-emitted from the trap. This radiation can be captured by a lens and focused onto a photodiode, producing an analog voltage as a useful diagnostic. The difference between

peak and steady-state voltage after the pulse is a direct probe of the atomic population. This technique is generally employed only as a diagnostic tool for fast readout when optimizing the alignment of cooling and trapping beams, and as such will not be discussed in further detail. The second optical interrogation technique, resonant absorprtion imaging, is only available in the upstairs laboratory. Therefore the theory, construction, and use of the absorption imaging apparatus is discussed in Chapter **??**.

Single-atom detection with the MCP-DLD stack

The principal detection scheme in this thesis is single-atom sensing in the far-field regime using a multichannel plate and delay-line detector combination (MCP-DLD). In some experiments, such as those conducted by the He* group at VU Amsterdam, the MCP itself can be used as an ion- or metastable-atom detector. In our experiments, the MCP is paired with either a phosphor screen (usually only used for diagnostic purposes) or with a delay line detector to form the MCP-DLD, which is the workhorse of most experiments conducted at ANU. A summary description is given here, and detailed explanations of the detector stack and signal processing pipeline can be found in [**ShinThesis**, 44, 59]. The MCP consists of two plates, each of which feature 30μm-diameter pores arranged in a square grid with 60μm between the centres of the pore openings. The plates are 80mm in diameter and mounted on an 8" vacuum flange, with the upper surface 848mm below the BiQUIC trap centre. The freefall time-of-flight of the centre of mass of the cloud is 417ms, which means the maximum measurable horizontal velocity is about 9.5 m/s. This provides a field-of-view that of about $\pm 6\ \mu\text{m}^{-1}$ in reciprocal space, sufficient to capture almost all of the thermal fraction for clouds below the critical temperature. The detector plates are grounded for most of the experimental sequence, and then the top plate is ramped to -2.4kV over about 2 seconds before dropping the trap. The negative voltage repels electrons from the surface of the plate which protects the detector surface from degradation and reduces the background count rate. The background rate, also called the *dark count* rate, is 0.56 Hz/cm^2 when opearting at -2.4kV, which is practically negligible for the purposes of experiments in this thesis.

When an atom strikes the surface of a pore after falling from the trap, a second-order process releases an electron with most of the 19.8eV as kinetic energy[**ThatPaper**]. These electrons are accelerated down the pore by the strong electric field, and themselves impact the pore surface and eject more electrons, triggering an electron avalanche that amplifies each atom impact into some 10^6 electrons. The electron shower exits the back of the detector and is accelerated by a +300V potential towards the delay-line detector (DLD). The DLD in the BiQUIC machine consists of two coils of wire each wound in a helical pattern and arranged perpendicular to one another. The arrival of an electron cascade causes a current pulse to travel along each wire in both directions from the point of impact. The pulses pass through a fast pre-amplifier and then through a constant-fraction discriminator which converts the analog pulses into a digital signal. Both these processes take place within a Roentdek DLATR6 which is located outside the vacuum chamber. The digital pulses are transmitted to a Roentdek TDC8HP time-digital converter (TDC) which registers the arrival time, relative to the arrival of the main trigger signal from the LabView control software, and writes these to a `*d.txt` file as `(channel,time)` pairs. The `*` is replaced by the current value of a counter tracking the number of experimental cycles (or *shots*) taken so far. Finally, a custom C++ script passes over the file and converts the timing data to `(t,x,y)` tuples. The conversion from `(channel,time)` to `(t,x,y)` is performed separately, and indeed the latter usually by a different machine, so as to provide maximum CPU availability to the acquisition function. Further details about the architecture, construction, and calibration of these detectors is found in [**DallThesis**, 44, 59].

A second MCP, backed by a phosphor screen and a mirror at 45° to the vertical axis, is mounted on an in-vacuum translation stage below the main chamber. The mirror directs light from the phosphor screen to a CCD camera mounted outside the vacuum chamber. This detection method is not typically used for scientific purposes, but is a useful additional

diagnostic when the MCP-DLD detector stack appears to be faulty. The phosphor screen does have a much larger dynamic range than the DLD, however, which makes it useful for visual spotting of subtle distortions in the BEC profile, such as used in the alignment of the spectroscopic probe beam, as described in chapter **??**.

Atom lasers

The most straightforward way to use an MCP-DLD to interrogate a BEC is simply to drop the atoms onto the detector. An example of this straightforward detection scheme is illustrated in Fig. 2.4. A drawback of this method is that the high atom fluxes in large BECs can temporarily deplete the available current carriers near the surface of the detector, resulting in a nonlinear reduction in detection efficiency known as *saturation*. This means that for even moderately sized condensates, a determination of the condensate population by counting detection events or by straightforward fitting of the time-of-flight profile is impractical, and one cannot compute interesting quantities like correlation functions with meaningful accuracy. Another limitation of the trap-release method is that it is a completely destructive measurement - one cannot re-trap the cloud or only drop part of it, which slows down data acquisition for even simple purposes like determining the trapping frequencies. Atom laser methods can circumvent both of these issues.

The basic principle of an atom laser is to transfer some portion of the condensed atoms into a state that is no longer confined by the trapping potential. This was first achieved by applying pulses of RF radiation to a magnetically trapped condensate shortly after their first realization [64]. Later, a continuous-wave atom laser was demonstrated and used to perform RF spectroscopy of the cloud, revealing the symmetry-breaking action of gravity which pulls the BEC away from the minimum of the magnetic field [10]. Optical Raman transitions[8] can also be used as the outcoupling mechanism [34] with the advantage of imparting a controllable momentum to the outcoupled atoms, but are not employed in the works in this thesis.

Atom lasers are so named because the trapped condensate acts as a reservoir of coherent matter waves, in analogy to lasers as a source of coherent light. The detailed correlation statistics of coherent light, as first detailed by Glauber [**glauberXX**], differ from BECs, as although they are both described by bosonic quantum fields, the commutation relations are different. This implications are discussed in [**narashewski**]. Nonetheless, the first-order coherence of atom lasers is evident from the observation of interference fringes between matter-wave beams [5] and the higher-order coherence manifests in the many-particle correlations detected in He* atom lasers [**SomeMorePapers**]. Atom lasers can also be collimated [10], directed with collimated laser beams playing the analogous role of an optical waveguide [33, 17], and manipulated with optically-induced 'mirrors' and beamsplitters [11]. The potentially continuous operation of atom lasers [**Chikkatur02**] brings the analogy with conventional lasers even closer. Atom laser physics has been studied in detail and widely deployed through the field of atom optics in the two intervening decades since their conception, and are instrumental for the works described in this thesis.

A simple explanation of the mechanism of an atom laser requires a two-level atom with magnetically trapped and untrapped states labeled $|1\rangle$ and $|0\rangle$. An RF pulse tuned to the splitting ω_{10} for a duration t induces an oscillation between the two states with Rabi frequency Ω. For an ensemble of N atoms, the independent single-particle oscillations produce a many-body state which evolves as [64]

$$(\cos(\Omega t/2)|0\rangle + \sin(\Omega t/2)|1\rangle)^{\otimes N} = \sum_{n=0}^{N} \sqrt{\frac{N!}{n!(N-n)!}} \cos(\Omega t/2)^{N-n} \sin(\Omega t/2)^{n} |N-n, n\rangle, \tag{2.1}$$

[8] In atom optics, *Bragg* transitions, which impart a momentum transfer, are distinguished from *Raman* transitions which also induce a change in the electronic state.

where $|N-n, n\rangle$ denotes the state with n atoms coupled out of the trapped state and $N-n$ atoms remaining. The outcoupled fraction is then $\sin^2(\Omega t/2)$.

In practise, the Zeeman splitting varies across the trap, and so a narrow RF pulse would only be resonant with a section of the condensate. While considering detailed spectroscopy of the condensate, this can be circumvented by applying short RF pulses resonant with the minimum Zeeman splitting of the trap. If such pulses are sufficiently short, the Fourier broadening of the finite-duration pulse is wider than the RF width of the condensate. The typical radio-frequency width of the condensate, i.e. the difference between the resonant frequency at the centre and the edge of the condensate, is set by the chemical potential of the condensate and is typically less than 10kHz in our experiments. An example of the MCP-DLD readout from a pulsed atom laser is shown in Figure 2.5.

2.4 Vacuum system integration

While nature abhors a vacuum, experimentalists abhor a background. Ultracold atom experiment require ultra-high vacuum (UHV) conditions because collisions with a background gas can easily overcome the frail forces that hold the atoms in their traps. Our vacuum is maintained by continuous operation of several turbomolecular pumps[9], which are backed by roughing pumps. Contamination of the vacuum chamber interior occurs from environmental sources like atmospheric pollutants or errors while handling components. When first pumping down to vacuum, contamination by water, oils, dust, or other materials can prevent achievement of good vacuum because of outgassing of volatile chemicals within the contaminant. These surface contaminants can be removed by wrapping the machine in heater tapes and insulating aluminium foil, and baking at 150-200 degrees celsius for several days. In this process one typically observes a sharp rise in pressure as the chamber heats and the contaminants volatalize, and then a decrease to a lower steady-state pressure as the contaminants cease outgassing and the remnants are evacuated. Once the pressure stabilizes, the heater tapes can be turned off, and as the apparatus cools the pressure will settle to a more preferable level. Care must be taken not to heat or cool the machine too quickly, or differences in thermal expansion between connected flanges can open leaks to atmosphere and undo much patient work.

Even after baking, the pressure may not be low enough to permit long-lived traps. Hydrogen leaching from the surface of the steel chamber can be significant. One method of dealing with this is by titanium sublimation. Specialized 'titanium sublimation pumps' pass a large current (several amps, pulsed) through a titanium filament which sublimates titanium atoms that eventually adsorbs on the walls of the chamber. Hydrogen adsorbs to the titanium surface but not to steel, and so after some applications the pressure trends further down. Further reduction in hydrogen background can be achieved by so-called 'getters', which present a highly porous surface into the vacuum and to which Hydrogen is strongly adsorbed. The chemical makeup of the background pressure can be determined using residual gas analysers (RGAs) which are essentially compact mass spectrometers. They can help diagnose whether one has an air leak or organic contaminant, and are helpful for leak hunting when paired with a bottle of helium gas, gently vented near suspect flanges.

The vacuum systems form the skeleton of both machines, which have a common structure illustrated schematically in 2.6. The placement of some of the turbomolecular pumps, faraday cups, and pressure gauges differ between the machines, but this makes no functional difference. However, the beamline of Staggering Grace does not feature a deflection stage or a focus for the LVIS. Otherwise, the overall structure of the vacuum systems is the same and so only Cacophanous Harmony is shown in its entirety in in Figure 2.6.

A major difference between the two setups is the construction of the chamber housing the final trapping stage, fondly known as the 'science chamber', in which BEC is achieved. Cacophanous Harmony has more limited optical access and has featured the spectroscopic laser, as depicted in Figure 2.6. For comparison, the apparatus around Staggering Grace's science chamber is shown and described in Chapter ??.

2.5 Data acquisition & control

Control of the optical components (AOMs and shutters), coil current supplies, and RF radiation is coordinated by a central LabView program which transmits pulse sequences to the machine via National Instruments pulse cards. The cards themselves are connected to the CPU by a PCI bus, and synchronize their internal clocks at the beginning of each shot.

[9] One of the earliest accomplishments of significant vacuum was by Lavoisier, who used pumps from the firestation to evacuate a chamber. Since then vacuum has advanced considerably, and at ultrahigh vacuum the exhaust is so dilute that one does not have the viscosity to operate pumps in the true sense. Nonetheless, the name remains.

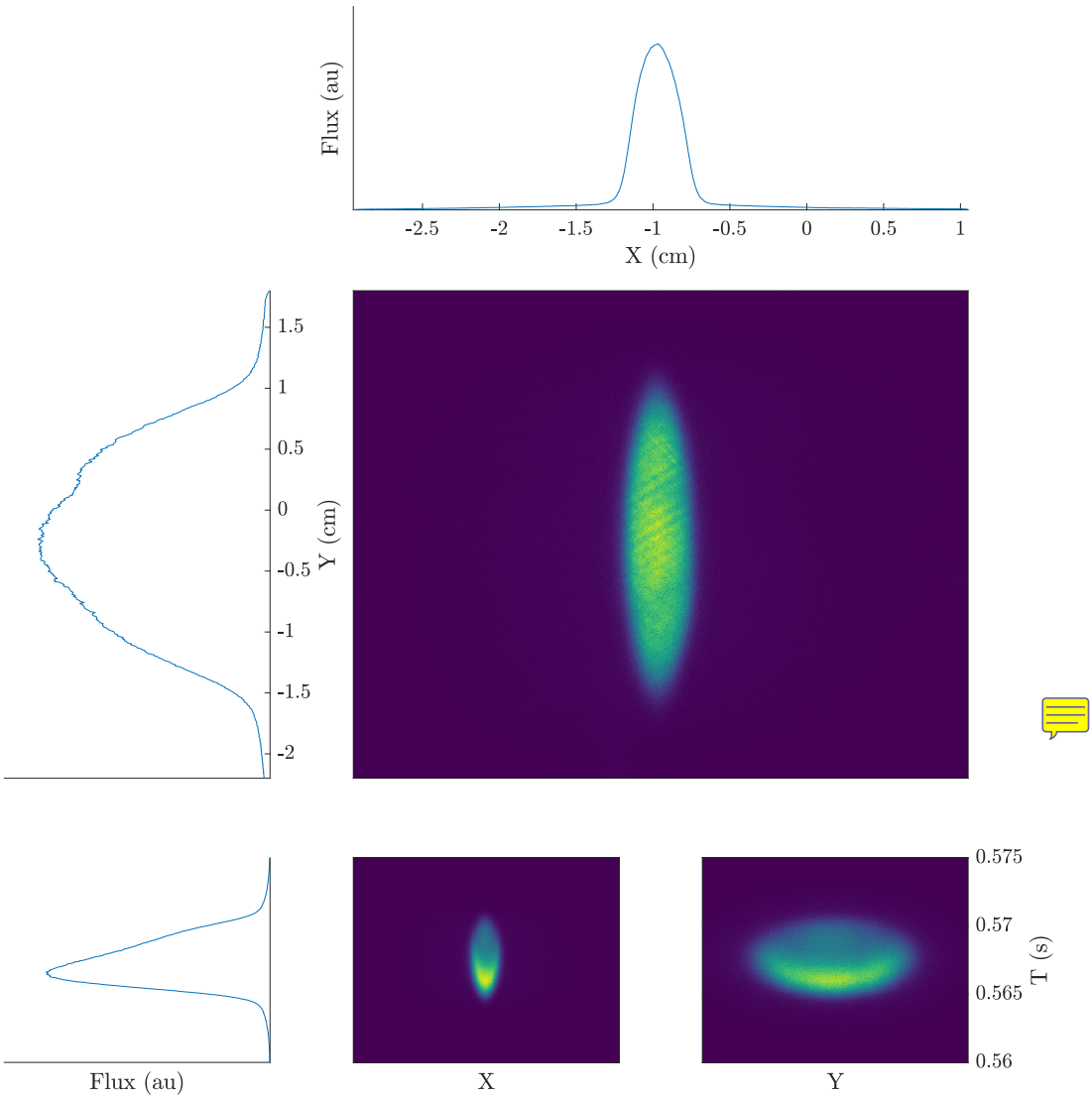

Figure 2.4: MCP readout of a dropped BEC with small thermal fraction. The detector saturation is evident in the time-of-flight profiles (bottom row) as a sudden downturn in the detected flux, whereas the full BEC has a parabolic profile. The density- and space-dependence of the saturation is visible in the 2D sections (lower middle and lower right).

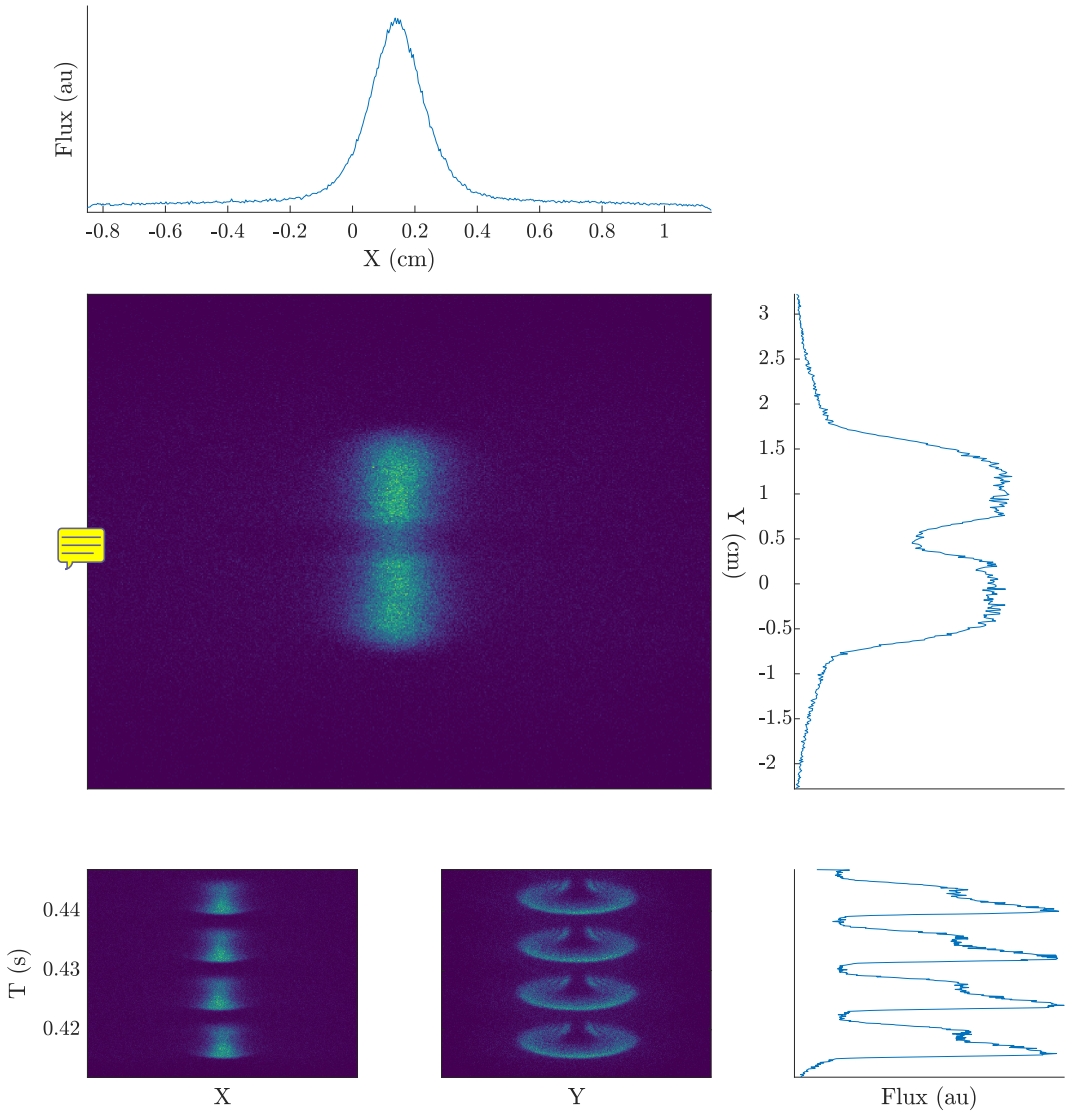

Figure 2.5: MCP readout of the first few pulses from a pulsed atom laser.

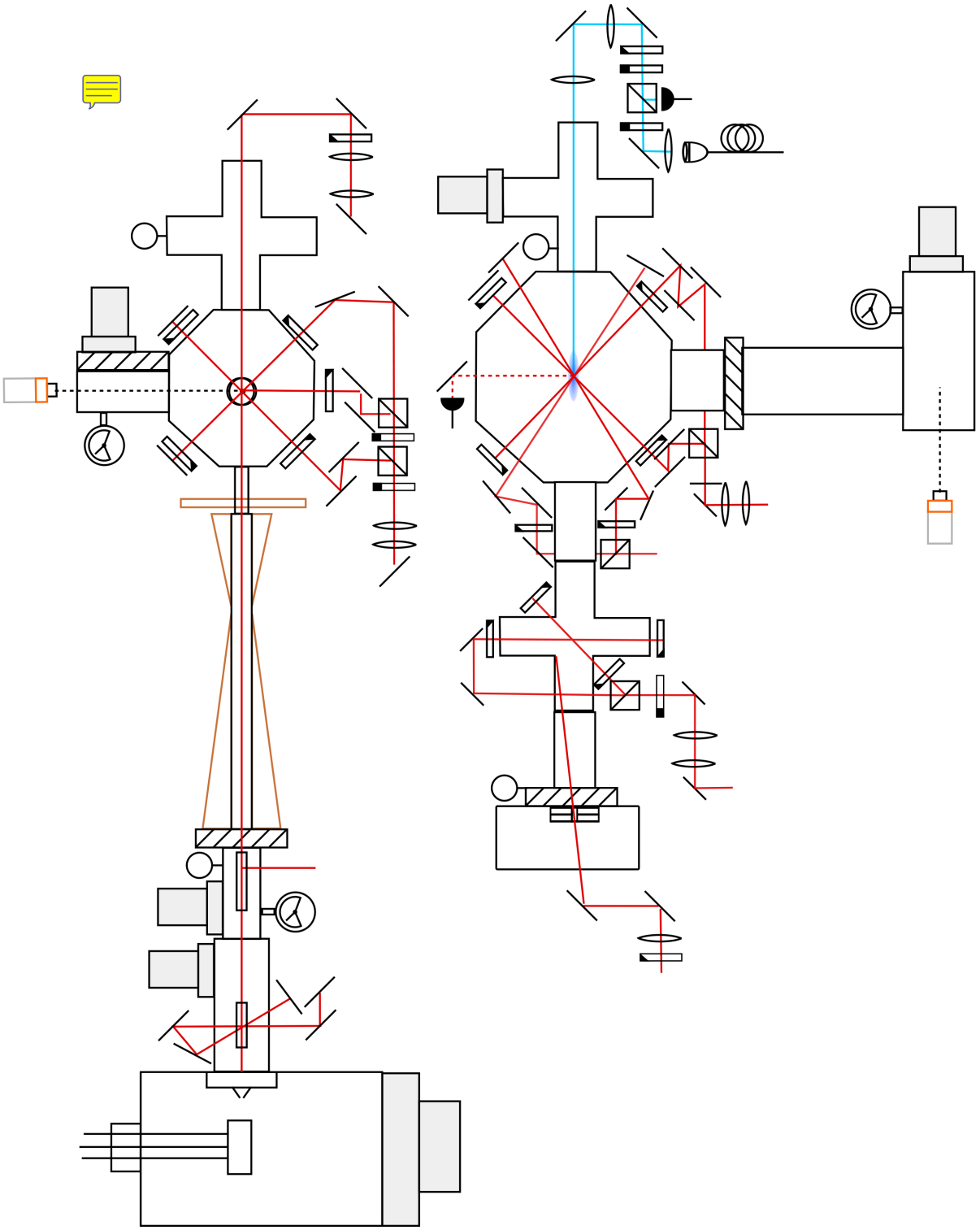

Figure 2.6: Vacuum system and laser insertion optics used in the downstairs experiment

The cards also record analog inputs such as Fabry-Perot cavity scan traces, photodiode traces, and mains voltage traces for post-processing diagnostics.

The LabView software is old, and the absence of documentation made significant modifications impractical. A workaround was accomplished by including a command that calls a specified MATLAB subroutine (referred to as the 'interface'), which is customizable to suit the purposes of a given experiment[10]. This subroutine can pass a `.xml` file path to a LabView pulse sequence file to use in the next experimental cycle, and even modify the sequences, albeit in a limited way due to the particulars of LabView's sequence specification format. This extension allows for automatic optimization of experimental sequences, as was demonstrated in [**HensonML**], but obviously is of no use for mechanical tasks like beam alignment[11]. The interface script also writes metadata to a log file, including the POSIX timestamp, type of shot executed (e.g. `calibration` or `AtomLaser`), shot number, and other relevant parameters. The timestamps in this logfile can be cross-referenced with the `*d.txt` files that are written by the TDC computer and with the LabView logs of analog inputs in order to match the experimental parameters with data files for post-processing purposes. The data analysis pipelines for modern experiments can be complex, and the experiments in this thesis generally comprise a handful of different diagnostics processed in parallel. The tagging of shots by timestamp cross-referencing allows separation of relevant shots for each processing subroutine. An example of the detailed diagnostics produced from the logs and metadata are shown in Figure X diagnostic figure

A more elegant solution could take the form of a main script that generates control pulses, absorbs the functions of the interface while monitoring the TDC output directory, and creates a direct link between log files and the `d.txt` files. Unfortunately, even if LabView were able to provide all this functionality, upgrading the control software would be like moving deckchairs on the titanic. It would be more effective to replace the entire control suite, which could take several months. Given the long build times required for new experiments, during which continuous operability is essential, and that adjusting the control software is a relatively small part of the demands of operator time, this upgrade is not a high priority. However, the control software for Staggering Grace was recently upgraded to a more readily usable and modifiable Python based infrastructure, which will surely prove both helpful and informative for future designs.

[10] The software developed to analyse the data from various experiments is invariably written in MATLAB. Many core capabilities are stored in the repository `https://github.com/HeBECANU/Core_BEC_Analysis`, and generally each project will have a unique public repository as well.

[11] One can dream, though.

Bibliography

[1] A list of sources is found at plasma-universe.com.

[2] See https://www.bose.res.in/Conferences/BECRP18/Mukunda.pdf and references therein.

[3] Admittedly, to my knowledge, this has yet to be detected.

[4] A. H. Abbas et al. "Rapid generation of metastable helium Bose-Einstein condensates". en. In: *arXiv:2102.10810 [cond-mat]* (Feb. 2021). arXiv: 2102.10810. URL: http://arxiv.org/abs/2102.10810 (visited on 03/11/2021).

[5] M R Andrews et al. "Observation of Interference Between Two Bose Condensates". In: *Science* 275 (1997), pp. 637–641.

[6] M. D. Barrett, J. A. Sauer, and M. S. Chapman. "All-Optical Formation of an Atomic Bose-Einstein Condensate". In: *Phys. Rev. Lett.* 87 (1 June 2001), p. 010404. DOI: 10.1103/PhysRevLett.87.010404. URL: https://link.aps.org/doi/10.1103/PhysRevLett.87.010404.

[7] Gordon Baym, Christopher Pethick, and David Pikes. "Superfluidity in Neutron Stars". In: *Nature* 224.5220 (Nov. 1969), pp. 673–674. ISSN: 0028-0836, 1476-4687. DOI: 10.1038/224674a0. URL: http://www.nature.com/articles/224674a0.

[8] K L Bell, A Dalgarno, and A E Kingston. "Penning ionization by metastable helium atoms". In: *Journal of Physics B: Atomic and Molecular Physics* 1 (1968).

[9] James Binney and David Skinner. *The Physics of Quantum Mechanics*. Capella Archive, 2008.

[10] Immanuel Bloch, Theodor W. Hänsch, and Tilman Esslinger. "Atom Laser with a cw Output Coupler". In: *Phys. Rev. Lett.* 82 (15 Apr. 1999), pp. 3008–3011. DOI: 10.1103/PhysRevLett.82.3008. URL: https://link.aps.org/doi/10.1103/PhysRevLett.82.3008.

[11] Immanuel Bloch et al. "Optics with an Atom Laser Beam". In: *Phys. Rev. Lett.* 87 (3 July 2001), p. 030401. DOI: 10.1103/PhysRevLett.87.030401. URL: https://link.aps.org/doi/10.1103/PhysRevLett.87.030401.

[12] J. S. Borbely et al. "Magnetic-field-dependent trap loss of ultracold metastable helium". In: *Phys. Rev. A* 85 (2 Feb. 2012), p. 022706. DOI: 10.1103/PhysRevA.85.022706. URL: https://link.aps.org/doi/10.1103/PhysRevA.85.022706.

[13] D. M. Brink and C. V. Sukumar. "Majorana spin-flip transitions in a magnetic trap". In: *Phys. Rev. A* 74 (3 Sept. 2006), p. 035401. DOI: 10.1103/PhysRevA.74.035401. URL: https://link.aps.org/doi/10.1103/PhysRevA.74.035401.

[14] L J Byron et al. "Suppression of Penning ionization in a spin-polarized mixture of rubidium and He *". en. In: *New Journal of Physics* 12.1 (Jan. 2010), p. 013004. ISSN: 1367-2630. DOI: 10.1088/1367-2630/12/1/013004. URL: https://iopscience.iop.org/article/10.1088/1367-2630/12/1/013004 (visited on 03/11/2021).

[15] L. J. Byron, R. G. Dall, and A. G. Truscott. "Trap loss in a metastable helium-rubidium magneto-optical trap". en. In: *Physical Review A* 81.1 (Jan. 2010), p. 013405. ISSN: 1050-2947, 1094-1622. DOI: 10.1103/PhysRevA.81.013405. URL: https://link.aps.org/doi/10.1103/PhysRevA.81.013405 (visited on 03/11/2021).

[16] Ph. W. Courteille, V. S. Bagnato, and V. I. Yukalov. "Bose-Einstein Codnensation of Trapped Atomic Gases". In: (2001). eprint: cond-mat/0109421.

[17] A Couvert et al. "A quasi-monomode guided atom laser from an all-optical Bose-Einstein condensate". In: *Europhysics Letters* 83 (2008), p. 50001.

[18] Franco Dalfovo et al. "Theory of Bose-Einstein condensation in trapped gases". In: *Rev. Mod. Phys.* 71 (3 1999), pp. 463–512. DOI: 10.1103/RevModPhys.71.463. URL: https://link.aps.org/doi/10.1103/RevModPhys.71.463.

[19] R. G. Dall, C. J. Dedman, and A. G. Truscott. "Feedback control of an atom laser". en. In: *Optics Express* 16.19 (Sept. 2008), p. 14716. ISSN: 1094-4087. DOI: 10.1364/OE.16.014716. URL: https://www.osapublishing.org/oe/abstract.cfm?uri=oe-16-19-14716 (visited on 03/11/2021).

[20] R. G. Dall et al. "Experimental Determination of the Helium 2 P 1 3 – 1 S 0 1 Transition Rate". en. In: *Physical Review Letters* 100.2 (Jan. 2008), p. 023001. ISSN: 0031-9007, 1079-7114. DOI: 10.1103/PhysRevLett.100.023001. URL: https://link.aps.org/doi/10.1103/PhysRevLett.100.023001 (visited on 03/11/2021).

[21] R. G. Dall et al. "Ideal n-body correlations with massive particles". en. In: *Nature Physics* 9.6 (June 2013), pp. 341–344. ISSN: 1745-2473, 1745-2481. DOI: 10.1038/nphys2632. URL: http://www.nature.com/articles/nphys2632 (visited on 03/11/2021).

[22] R. G. Dall et al. "Observation of the first excited transverse mode in guided matter waves". en. In: *Optics Letters* 36.7 (Apr. 2011), p. 1131. ISSN: 0146-9592, 1539-4794. DOI: 10.1364/OL.36.001131. URL: https://www.osapublishing.org/abstract.cfm?URI=ol-36-7-1131 (visited on 03/11/2021).

[23] R. G. Dall et al. "Transverse mode imaging of guided matter waves". en. In: *Physical Review A* 81.1 (Jan. 2010), p. 011602. ISSN: 1050-2947, 1094-1622. DOI: 10.1103/PhysRevA.81.011602. URL: https://link.aps.org/doi/10.1103/PhysRevA.81.011602 (visited on 03/11/2021).

[24] R.G. Dall and A.G. Truscott. "Bose–Einstein condensation of metastable helium in a bi-planar quadrupole Ioffe configuration trap". In: *Optics Communications* 270.2 (Feb. 2007), pp. 255–261. DOI: 10.1016/j.optcom.2006.09.031. URL: http://dx.doi.org/10.1016/j.optcom.2006.09.031.

[25] R.G. Dall et al. "Observation of atomic speckle and Hanbury Brown–Twiss correlations in guided matter waves". en. In: *Nature Communications* 2.1 (Sept. 2011), p. 291. ISSN: 2041-1723. DOI: 10.1038/ncomms1292. URL: http://www.nature.com/articles/ncomms1292 (visited on 03/11/2021).

[26] K B Davis et al. "Bose-Einstein condensation in a gas of sodium atoms". In: *Physical Review Letters* 75 (1995), pp. 3969–3973. DOI: https://doi.org/10.1103/PhysRevLett.75.3969.

[27] C J Dedman et al. "Precision temperature controlled filtered laminar air enclosure". en. In: *Measurement Science and Technology* 26.2 (Feb. 2015), p. 027002. ISSN: 0957-0233, 1361-6501. DOI: 10.1088/0957-0233/26/2/027002. URL: https://iopscience.iop.org/article/10.1088/0957-0233/26/2/027002 (visited on 03/11/2021).

[28] C. J. Dedman et al. "Optimum design and construction of a Zeeman slower for use with a magneto-optic trap". en. In: *Review of Scientific Instruments* 75.12 (Dec. 2004), pp. 5136–5142. ISSN: 0034-6748, 1089-7623. DOI: 10.1063/1.1820524. URL: http://aip.scitation.org/doi/10.1063/1.1820524 (visited on 03/11/2021).

[29] C J Foot. *Atomic Physics*. Oxford university press, 2005.

[30] J Ginibre. "On th asymptotic exactness of the Bogoliubov approximation for many boson systems". In: *Communications in Mathematical Physics* 8 (1967), pp. 26–51. DOI: 10.1007/BF01646422.

[31] M. R. Goosen et al. "Feshbach resonances in ^{3}He*-^{4}He* mixtures". In: *Phys. Rev. A* 82 (4 Oct. 2010), p. 042713. DOI: 10.1103/PhysRevA.82.042713. URL: https://link.aps.org/doi/10.1103/PhysRevA.82.042713.

[32] Rudolf Grimm, Matthias Weidemüller, and Yurii B. Ovchinnikov. "Optical Dipole Traps for Neutral Atoms". In: ed. by Benjamin Bederson and Herbert Walther. Vol. 42. Advances In Atomic, Molecular, and Optical Physics. Academic Press, 2000, pp. 95–170. DOI: https://doi.org/10.1016/S1049-250X(08)60186-X. URL: http://www.sciencedirect.com/science/article/pii/S1049250X0860186X.

[33] W. Guerin et al. "Guided Quasicontinuous Atom Laser". In: *Phys. Rev. Lett.* 97 (20 Nov. 2006), p. 200402. DOI: 10.1103/PhysRevLett.97.200402. URL: https://link.aps.org/doi/10.1103/PhysRevLett.97.200402.

[34] E W Hagley et al. "A Well-Collimated Quasi-Continuous Atom Laser". In: *Science* 283 (1999), pp. 1706–1709.

[35] B. Haskell and A. Sedrakian. "Superfluidity and Superconductivity in Neutron Stars". In: *The Physics and Astrophysics of Neutron Stars*. Ed. by L Rezzolla et al. Astrophysics and Space Science Library, 2018, pp. 401–454. DOI: https://doi.org/10.1007/978-3-319-97616-7_8.

[36] B. M. Henson et al. "Bogoliubov-Cherenkov radiation in an atom laser". In: *Physical Review A* 97.6 (June 2018). DOI: 10.1103/physreva.97.063601. URL: http://dx.doi.org/10.1103/PhysRevA.97.063601.

[37] B. M. Henson et al. "Precision Measurement for Metastable Helium Atoms of the 413 nm Tune-Out Wavelength at Which the Atomic Polarizability Vanishes". In: *Phys. Rev. Lett.* 115 (4 July 2015), p. 043004. DOI: 10.1103/PhysRevLett.115.043004. URL: https://link.aps.org/doi/10.1103/PhysRevLett.115.043004.

[38] N. Herschbach et al. "Photoassociation Spectroscopy of Cold He(2^3S) Atoms". In: *Phys. Rev. Lett.* 84 (9 Feb. 2000), pp. 1874–1877. DOI: 10.1103/PhysRevLett.84.1874. URL: https://link.aps.org/doi/10.1103/PhysRevLett.84.1874.

[39] S. S. Hodgman et al. "Direct Measurement of Long-Range Third-Order Coherence in Bose-Einstein Condensates". en. In: *Science* 331.6020 (Feb. 2011), pp. 1046–1049. ISSN: 0036-8075, 1095-9203. DOI: 10.1126/science.1198481. URL: https://www.sciencemag.org/lookup/doi/10.1126/science.1198481 (visited on 03/11/2021).

[40] S. S. Hodgman et al. "Higher-Order Quantum Ghost Imaging with Ultracold Atoms". en. In: *Physical Review Letters* 122.23 (June 2019), p. 233601. ISSN: 0031-9007, 1079-7114. DOI: 10.1103/PhysRevLett.122.233601. URL: https://link.aps.org/doi/10.1103/PhysRevLett.122.233601 (visited on 03/11/2021).

[41] S. S. Hodgman et al. "Metastable Helium: A New Determination of the Longest Atomic Excited-State Lifetime". In: *Physical Review Letters* 103.5 (July 2009). DOI: 10.1103/physrevlett.103.053002. URL: http://dx.doi.org/10.1103/PhysRevLett.103.053002.

[42] S. S. Hodgman et al. "Metastable Helium: A New Determination of the Longest Atomic Excited-State Lifetime". en. In: *Physical Review Letters* 103.5 (July 2009), p. 053002. ISSN: 0031-9007, 1079-7114. DOI: 10.1103/PhysRevLett.103.053002. URL: https://link.aps.org/doi/10.1103/PhysRevLett.103.053002 (visited on 03/11/2021).

[43] S. S. Hodgman et al. "Solving the Quantum Many-Body Problem via Correlations Measured with a Momentum Microscope". In: *Phys. Rev. Lett.* 118 (24 June 2017), p. 240402. DOI: 10.1103/PhysRevLett.118.240402. URL: https://link.aps.org/doi/10.1103/PhysRevLett.118.240402.

[44] Sean Stewart Hodgman. "Transition Lifetime Measurements and Correlation Experiments with Ultra-cold Metastable Helium". en. In: (), p. 184.

[45] E A Hylleraas. "Neue berechnung der Energie des Heliums im Grunzustande, soqie des tiefsten Terms von Ortho-helium". In: *Z Physik* (54 1929).

[46] E A Hylleraas. "Uber den grundzustand des Heliumatoms". In: *Z Physik* (48 1920).

[47] E A Hylleraas and B Undheim. "Numerische berechnun der 2S terme von Ortho- und Par-helium". In: *Z Physik* (65 1930).

[48] Koelemeij J C J et al. "High densities and optical collisions in a two-colour magneto-optical trap for metastable helium". In: *Journal of Physics B: Atomic, Molecular and Optical physics* (37 2004), p. 3501.

[49] T Jeltes et al. "Comparison of the Hanbury Brown-Twiss effect for bosons and fermions". In: *Nature* 445 (2007). DOI: doi:10.1038/nature05513.

[50] W. Ketterle, D. S. Durfee, and D. M. Stamper-Kurn. "Making, probing, and understanding Bose-Einstein condensates". In: (1999). eprint: cond-mat/9904034.

[51] R. I. Khakimov et al. "Ghost imaging with atoms". In: *Nature* 540 (2016). DOI: doi.org/10.1038/nature20154.

[52] M. A. Kristensen et al. "Observation of Atom Number Fluctuations in a Bose-Einstein Condensate". In: *Phys. Rev. Lett.* 122 (16 Apr. 2019), p. 163601. DOI: 10.1103/PhysRevLett.122.163601. URL: https://link.aps.org/doi/10.1103/PhysRevLett.122.163601.

[53] P. J. Leo et al. "Ultracold collisions of metastable helium atoms". In: *Phys. Rev. A* 64 (2000), p. 042710. DOI: 10.1103/PhysRevA.64.042710.

[54] Müller M.W. et al. "Experimental and theoretical studies of the Bi-excited collision systems He*(23 S) + He*(23 S, 21 S) at thermal and subthermal kinetic energies". In: *Zeitschrift für Physik D Atoms, Molecules and Clusters* (21 1991), pp. 89–112. DOI: https://doi.org/10.1007/BF01425589.

[55] F. Manni et al. "Penrose-Onsager Criterion Validation in a One-Dimensional Polariton Condensate". In: *Phys. Rev. Lett.* 109 (15 2012), p. 150409. DOI: 10.1103/PhysRevLett.109.150409. URL: https://link.aps.org/doi/10.1103/PhysRevLett.109.150409.

[56] A G Manning et al. "Third-order spatial correlations for ultracold atoms". en. In: *New Journal of Physics* 15.1 (Jan. 2013), p. 013042. ISSN: 1367-2630. DOI: 10.1088/1367-2630/15/1/013042. URL: https://iopscience.iop.org/article/10.1088/1367-2630/15/1/013042 (visited on 03/11/2021).

[57] A. G. Manning et al. "Single-Atom Source in the Picokelvin Regime". en. In: *Physical Review Letters* 113.13 (Sept. 2014), p. 130403. ISSN: 0031-9007, 1079-7114. DOI: 10.1103/PhysRevLett.113.130403. URL: https://link.aps.org/doi/10.1103/PhysRevLett.113.130403 (visited on 03/11/2021).

[58] A. G. Manning et al. "The Hanbury Brown-Twiss effect in a pulsed atom laser". In: *Optics Express* 18.18 (Aug. 2010), p. 18712. DOI: 10.1364/oe.18.018712. URL: http://dx.doi.org/10.1364/OE.18.018712.

[59] Andrew Geoffrey Manning. "Foundation experiments in quantum atom optics with ultracold metastable helium". en. In: (), p. 193.

[60] R. I. Manning A G Khakimov, R G Dall, and A G Truscott. "Wheeler's delayed-choice gedanken experiment with a single atom". In: *Nature Physics* 11 (2015). DOI: https://doi.org/10.1038/nphys3343.

[61] Noël Martin and Michael Urban. "Superfluid hydrodynamics in the inner crust of neutron stars". In: *Phys. Rev. C* 94.6 (Dec. 2016), p. 065801. ISSN: 2469-9985, 2469-9993. DOI: 10.1103/PhysRevC.94.065801. URL: https://link.aps.org/doi/10.1103/PhysRevC.94.065801.

[62] J M McNamara et al. "Heteronuclear ionizing collisions between laser-cooled metastable helium atoms". In: *Physical Review A* (75 2007), p. 062715. DOI: 10.1103/PhysRevA.75.062715.

[63] Harold J. Metcalf and Peter van der Straten. *Laser Cooling and Trapping of Neutral Atoms*. Springer, 1999.

[64] M.-O. Mewes et al. "Output Coupler for Bose-Einstein Condensed Atoms". In: *Phys. Rev. Lett.* 78 (4 Jan. 1997), pp. 582–585. DOI: 10.1103/PhysRevLett.78.582. URL: https://link.aps.org/doi/10.1103/PhysRevLett.78.582.

[65] J. Mitroy and Li-Yan Tang. "Tune-out wavelengths for metastable helium". In: *Phys. Rev. A* 88 (5 Nov. 2013), p. 052515. DOI: 10.1103/PhysRevA.88.052515. URL: https://link.aps.org/doi/10.1103/PhysRevA.88.052515.

[66] S. Moal et al. "Accurate Determination of the Scattering Length of Metastable Helium Atoms Using Dark Resonances between Atoms and Exotic Molecules". In: *Phys. Rev. Lett.* 96.2 (Jan. 2006). DOI: 10.1103/physrevlett.96.023203. URL: https://journals.aps.org/prl/abstract/10.1103/PhysRevLett.96.023203.

[67] C Orzel et al. "Spin polarization and quantum-statistical effects in ultracold ionizing collisions". In: *Physical Review A* 59 (1999), pp. 1926–1935.

[68] Spoden P et al. "Collisional Properties of Cold Spin-Polarized Metastable Neon Atoms". In: *Physical Review Letters* 94 (2005).

[69] Dany Page et al. "Rapid Cooling of the Neutron Star in Cassiopeia A Triggered by Neutron Superfluidity in Dense Matter". In: *Phys. Rev. Lett.* (2011), p. 4. URL: https://journals.aps.org/prl/abstract/10.1103/PhysRevLett.106.081101.

[70] Oliver Penrose and Lars Onsager. "Bose-Einstein Condensation and Liquid Helium". In: *Phys. Rev.* 104 (3 Nov. 1956), pp. 576–584. DOI: 10.1103/PhysRev.104.576. URL: https://link.aps.org/doi/10.1103/PhysRev.104.576.

[71] C Pethick and H Smith. *Bose-Einstein condensation in dilute gases*. Cambridge University Press, 2002.

[72] L Pitaevskii and S Stringari. *Bose-Einstein Condensation*. Oxford University Publications, 2016.

[73] N. R. Poniatowski. "Superconductivity, broken gauge symmetry, and the Higgs mechanism". In: *American Journal of Physics* 87 (436 2019). DOI: 10.1119/1.5093291.

[74] M Przybytek and B Jeziorski. "Bounds for the scattering length of spin-polarized helium from high-accuracy electronic structure calculations". In: *Journal of Chemical Physics* (123 2005). DOI: https://doi.org/10.1063/1.2042453.

[75] R. J. Rengelink et al. "Precision spectroscopy of helium in a magic wavelength optical dipole trap". In: *Nature Physics* 14.11 (Aug. 2018), pp. 1132–1137. DOI: 10.1038/s41567-018-0242-5. URL: http://dx.doi.org/10.1038/s41567-018-0242-5.

[76] Jacob A. Ross et al. "Frequency measurements of transitions from the 2 P 2 3 state to the 5 D 2 1 , 5 S 1 3 , and 5 D 3 states in ultracold helium". en. In: *Physical Review A* 102.4 (Oct. 2020), p. 042804. ISSN: 2469-9926, 2469-9934. DOI: 10.1103/PhysRevA.102.042804. URL: https://link.aps.org/doi/10.1103/PhysRevA.102.042804 (visited on 03/11/2021).

[77] Wu RuGway et al. “Correlations in Amplified Four-Wave Mixing of Matter Waves”. en. In: *Physical Review Letters* 107.7 (Aug. 2011), p. 075301. ISSN: 0031-9007, 1079-7114. DOI: 10.1103/PhysRevLett.107.075301. URL: https://link.aps.org/doi/10.1103/PhysRevLett.107.075301 (visited on 03/11/2021).

[78] Wu RuGway et al. “Observation of Transverse Bose-Einstein Condensation via Hanbury Brown–Twiss Correlations”. en. In: *Physical Review Letters* 111.9 (Aug. 2013), p. 093601. ISSN: 0031-9007, 1079-7114. DOI: 10.1103/PhysRevLett.111.093601. URL: https://link.aps.org/doi/10.1103/PhysRevLett.111.093601 (visited on 03/11/2021).

[79] C C Bradleyand C A Sackett, J J Tollett, and G Hulet. “evidence of Bose-Einstein condesnation in an atomic gas with attractive interactions”. In: *physical review letters* 75 (1995), pp. 1687–1690. DOI: https://doi.org/10.1103/PhysRevLett.75.1687.

[80] M. Schellekens et al. “Hanbury Brown Twiss effect for ultracold quantum gases”. In: *Science* 310 (2005). DOI: 10.1126/science.1118024.

[81] Julian Schmitt et al. “Spontaneous Symmetry Breaking and Phase Coherence of a Photon Bose-Einstein Condensate Coupled to a Reservoir”. In: *Phys. Rev. Lett.* 116 (3 2016), p. 033604. DOI: 10.1103/PhysRevLett.116.033604. URL: https://link.aps.org/doi/10.1103/PhysRevLett.116.033604.

[82] Franz Schwabl. *Advanced Quantum Mechanics*. Trans. by R Hilton and A Lahee. Springer, 2000.

[83] D K Shin et al. “Entanglement-based 3D magnetic gradiometry with an ultracold atomic scattering halo”. en. In: *New Journal of Physics* 22.1 (Jan. 2020), p. 013002. ISSN: 1367-2630. DOI: 10.1088/1367-2630/ab66de. URL: https://iopscience.iop.org/article/10.1088/1367-2630/ab66de (visited on 03/11/2021).

[84] D. K. Shin et al. “Bell correlations between spatially separated pairs of atoms”. en. In: *Nature Communications* 10.1 (Dec. 2019), p. 4447. ISSN: 2041-1723. DOI: 10.1038/s41467-019-12192-8. URL: http://www.nature.com/articles/s41467-019-12192-8 (visited on 03/11/2021).

[85] G. V. Shlyapnikov et al. “Decay Kinetics and Bose Condensation in a Gas of Spin-Polarized Triplet Helium”. In: *Phys. Rev. Lett.* 73 (24 Dec. 1994), pp. 3247–3250. DOI: 10.1103/PhysRevLett.73.3247. URL: https://link.aps.org/doi/10.1103/PhysRevLett.73.3247.

[86] Robert P. Smith et al. “Effects of Interactions on the Critical Temperature of a Trapped Bose Gas”. In: *Phys. Rev. Lett.* 106 (25 June 2011), p. 250403. DOI: 10.1103/PhysRevLett.106.250403. URL: https://link.aps.org/doi/10.1103/PhysRevLett.106.250403.

[87] R J W Stas et al. “Homonuclear ionizing collisions of laser-cooled metastable helium atoms”. In: *Physical Review A* (73 2006), p. 032713. DOI: 10.1103/PhysRevA.73.032713.

[88] C. V. Sukumar and D. M. Brink. “Spin-flip transitions in a magnetic trap”. In: *Phys. Rev. A* 56 (3 Sept. 1997), pp. 2451–2454. DOI: 10.1103/PhysRevA.56.2451. URL: https://link.aps.org/doi/10.1103/PhysRevA.56.2451.

[89] András Sütő. “Equivalence of Bose-Einstein Condensation and Symmetry Breaking”. In: *Phys. Rev. Lett.* 94 (8 Mar. 2005), p. 080402. DOI: 10.1103/PhysRevLett.94.080402. URL: https://link.aps.org/doi/10.1103/PhysRevLett.94.080402.

[90] J.A. Swansson et al. “A high flux, liquid-helium cooled source of metastable rare gas atoms”. en. In: *Applied Physics B* 79.4 (Sept. 2004), pp. 485–489. ISSN: 0946-2171, 1432-0649. DOI: 10.1007/s00340-004-1600-9. URL: http://link.springer.com/10.1007/s00340-004-1600-9 (visited on 03/11/2021).

[91] Naaman Tammuz et al. "Can a Bose Gas Be Saturated?" In: *Phys. Rev. Lett.* 106 (23 June 2011), p. 230401. DOI: 10.1103/PhysRevLett.106.230401. URL: https://link.aps.org/doi/10.1103/PhysRevLett.106.230401.

[92] K. F. Thomas et al. "Direct measurement of the forbidden $2^3S_1 \rightarrow 3^3S_1$ atomic transition in helium". In: *Physical Review Letters* 125 (July 2020). DOI: https://doi.org/10.1103/PhysRevLett.125.013002. URL: https://journals.aps.org/prl/abstract/10.1103/PhysRevLett.125.013002.

[93] Paul J. J. Tol et al. "Large numbers of cold metastable helium atoms in a magneto-optical trap". In: *Phys. Rev. A* 60 (2 Aug. 1999), R761–R764. DOI: 10.1103/PhysRevA.60.R761. URL: https://link.aps.org/doi/10.1103/PhysRevA.60.R761.

[94] L. J. Uhlmann et al. "Electron Collisions with Laser Cooled and Trapped Metastable Helium Atoms: Total Scattering Cross Sections". en. In: *Physical Review Letters* 94.17 (May 2005), p. 173201. ISSN: 0031-9007, 1079-7114. DOI: 10.1103/PhysRevLett.94.173201. URL: https://link.aps.org/doi/10.1103/PhysRevLett.94.173201 (visited on 03/11/2021).

[95] V. Venturi et al. "Close-coupled calculation of collisions of magnetostatically trapped metastable helium atoms". In: *Phys. Rev. A* 60 (6 Dec. 1999), pp. 4635–4646. DOI: 10.1103/PhysRevA.60.4635. URL: https://link.aps.org/doi/10.1103/PhysRevA.60.4635.

[96] J. M. Vogels et al. "Experimental Observation of the Bogoliubov Transformation for a Bose-Einstein Condensed Gas". In: *Phys. Rev. Lett.* 88 (6 Jan. 2002), p. 060402. DOI: 10.1103/PhysRevLett.88.060402. URL: https://link.aps.org/doi/10.1103/PhysRevLett.88.060402.

[97] John Weiner et al. "Experiments and theory in cold and ultracold collisions". In: *Rev. Mod. Phys.* 71 (1 Jan. 1999), pp. 1–85. DOI: 10.1103/RevModPhys.71.1. URL: https://link.aps.org/doi/10.1103/RevModPhys.71.1.

[98] V. I. Yukalov. "Basics of Bose-Einstein condensation". In: *Physics of Particles and Nuclei* 42 (3 2011), pp. 460–513. DOI: 10.1134/S1063779611030063.

[99] V. I. Yukalov. "Bose-Einstein condensation and gauge symmetry breaking". In: *Laser physics letters* 4 (9 2007), pp. 632–647. DOI: 10.1002/lapl.200710029.